

Supporting Information

Carbazole-Functionalized Chichibabin Diradicaloids with Redshifted Absorption and Enhanced Photoluminescence

Vivek Chandrakant Wakchaure,^a Xingmao Chang,^a Julia Zolg,^{b,d} Rémi Blinder,^c
Mona E. Arnold,^b Fedor Jelezko,^{*c,d} Alexander J. C. Kuehne,^{*b,d} Max von Delius^{*a,d}

^a Institute of Organic Chemistry, Ulm University, Albert-Einstein-Allee 11, 89081 Ulm (Germany). E-mail:
max.vondelius@uni-ulm.de

^b Institute of Macromolecular and Organic Chemistry, Ulm University Albert-Einstein-Allee 11, 89081 Ulm (Germany). E-
mail: alexander.kuehne@uni-ulm.de

^c Institute of Quantum Optics, Ulm University Albert-Einstein-Allee 11, 89081 Ulm (Germany). E-mail: fedor.jelezko@uni-
ulm.de

^d Center for Integrated Quantum Science and Technology, Ulm University, Albert-Einstein-Allee 11, 89081 Ulm (Germany).

Contents

1. Materials and instrumentation	S3
2. Synthesis and characterisation of Cbz₂-TTM-TTM (1) and Cbz₂-TTM-TTM-Cbz₂ (2) .	S5
2.1 Synthesis of Cbz ₂ -HTTM	S5
2.2 Synthesis of Cbz ₂ -TTM-I.....	S6
2.3 Synthesis of 1 and 2	S8
2.4 Synthesis of Cbz ₂ -TTM-HTTM-Cbz ₂ (3).....	S10
3. Purification and HPLC-MS analysis.....	S11
5. Optical properties	S18
6. DFT calculations	S21
7. EPR measurements	S31
8. Supplementary NMR and mass spectra	S34
9. References.....	S43

1. Materials and instrumentation

All reagents and solvents were commercially available reagent quality unless indicated otherwise. Anhydrous solvents were dried before use in an MBraun SPS-800 instrument.

Thin layer chromatography (TLC) was conducted on pre-coated aluminum sheets with 0.20 mm Machevery-Nagel Alugram SIL G/UV254 with fluorescent indicator UV254 or 0.20 mm Merk Millipore Silica gel 60 with fluorescent indicator F254.

Column chromatography was carried out using Merck Gerduran silica gel 60 (particle size 40-63 μm).

Nuclear magnetic resonance (NMR) ^1H were obtained on a Bruker 400 MHz AVANCE or Bruker 600 MHz spectrometer and ^{13}C spectra at 150, or 100 MHz, in CDCl_3 , CD_2Cl_2 . Chemical shifts were reported in ppm according to tetramethyl silane using the solvent residual signal as an internal reference (CDCl_3 : $\delta_{\text{H}} = 7.26$ ppm, $\delta_{\text{C}} = 77.16$ ppm, CD_2Cl_2 : $\delta_{\text{H}} = 5.32$ ppm, $\delta_{\text{C}} = 53.84$ ppm, coupling constants (J) were given in Hz and were averaged. Resonance multiplicity was described as *s* (singlet), *d* (doublet), *t* (triplet), *m* (multiplet), *br* (broad signal), *dd* (doublet of doublets), *dt* (doublet of triplets). All spectra were recorded at 25 °C unless specified otherwise.

High resolution mass spectrometry (HRMS) was performed using a Fourier Transform Ion Cyclotron Resonance (FT-ICR) mass spectrometer solarix (Bruker Daltonik GmbH, Bremen, Germany) equipped with a 7.0 T superconducting magnet and interfaced to an Apollo II Dual ESI/MALDI source, which can be switched from ESI or APCI respectively to MALDI operation almost instantaneously. A trans-2-[3-(4-tertButylphenyl)-2-methyl-2-propenyldene]malononitrile (DCTB) used as a matrix.

Recycling GPC experiments were conducted on a LaboACE LC-7080 with a column JAIGEL-2HR Plus + 2.5 HR Plus; Eluent: Dichloromethane; Flow rate: 10 mL/min; Detector: UV-Vis 4ch LA @ 600-650 nm.

HPLC experiments were conducted on a Shimadzu 2020 HPLC-MS equipped with a Buckyprep M column.

The cyclic voltammetry (CV) measurements were performed on Bio-Logic SAS (SP-150).

UV-Vis absorption spectra were recorded on a Perkin Elmer Lambda 365 instrument.

Photoluminescence measurements were conducted with a PerkinElmer FL6500 instrument. Photoluminescence quantum yields (PLQYs) were obtained from Hamamatsu Quantaaurus-QY (C11347).

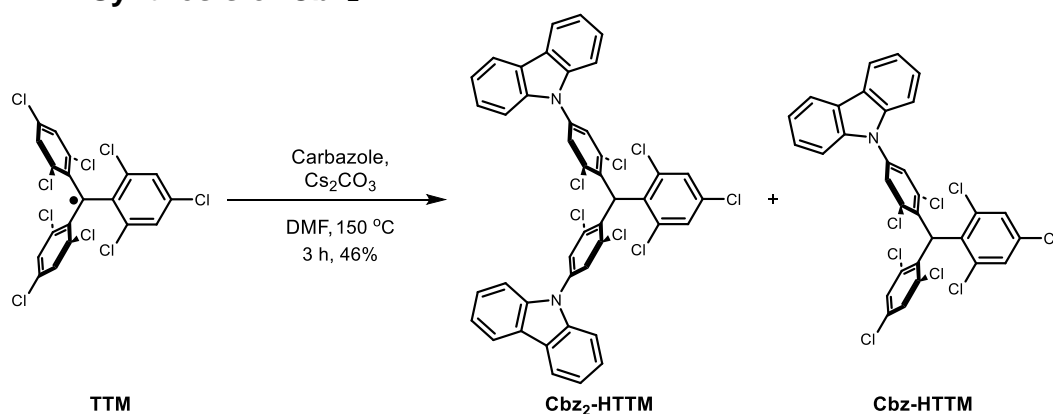
VT-EPR measurements were conducted on an X-band EPR system (Bruker ELEXSYS II E580), working in continuous wave (CW) mode, using the software xEPR from Bruker for acquisition. Measurements were taken with the ER4122 SHQE cavity. The ER4141VT system was used for control of the temperature down to 100 K, together with a quartz Dewar (Wilמד WG-821-STW-AH-Q) fitting inside the cavity. The cavity has a resonance quality factor $Q = 8000-10000$ (both with and without quartz Dewar). The microwave power produced by the EPR bridge is 150 mW. The power delivered to the resonator is adjusted by varying the attenuation at the output of the bridge, between 0 and 60 dB. Adjustment of this parameter was made to avoid the power saturation effect. Attenuation was set in between 39dB and

27dB (corresp. to power range 19-300 μ W) for the main transitions of diradicals. For the half-field transition (main text, Figure 4b) the power was increased to adapt to the different intensity and power saturation behavior of this transition: 0dB was used as attenuation, corresponding to 150 mW power.

The **TTM**, **HTTM-I**, and **TTM-I** precursors were synthesized according to literature reports.¹

2. Synthesis and characterisation of Cbz₂-TTM-TTM (1) and Cbz₂-TTM-TTM-Cbz₂ (2)

2.1 Synthesis of Cbz₂-HTTM



Scheme S1 Synthesis of Cbz₂-HTTM

Synthesis of Cbz₂-HTTM

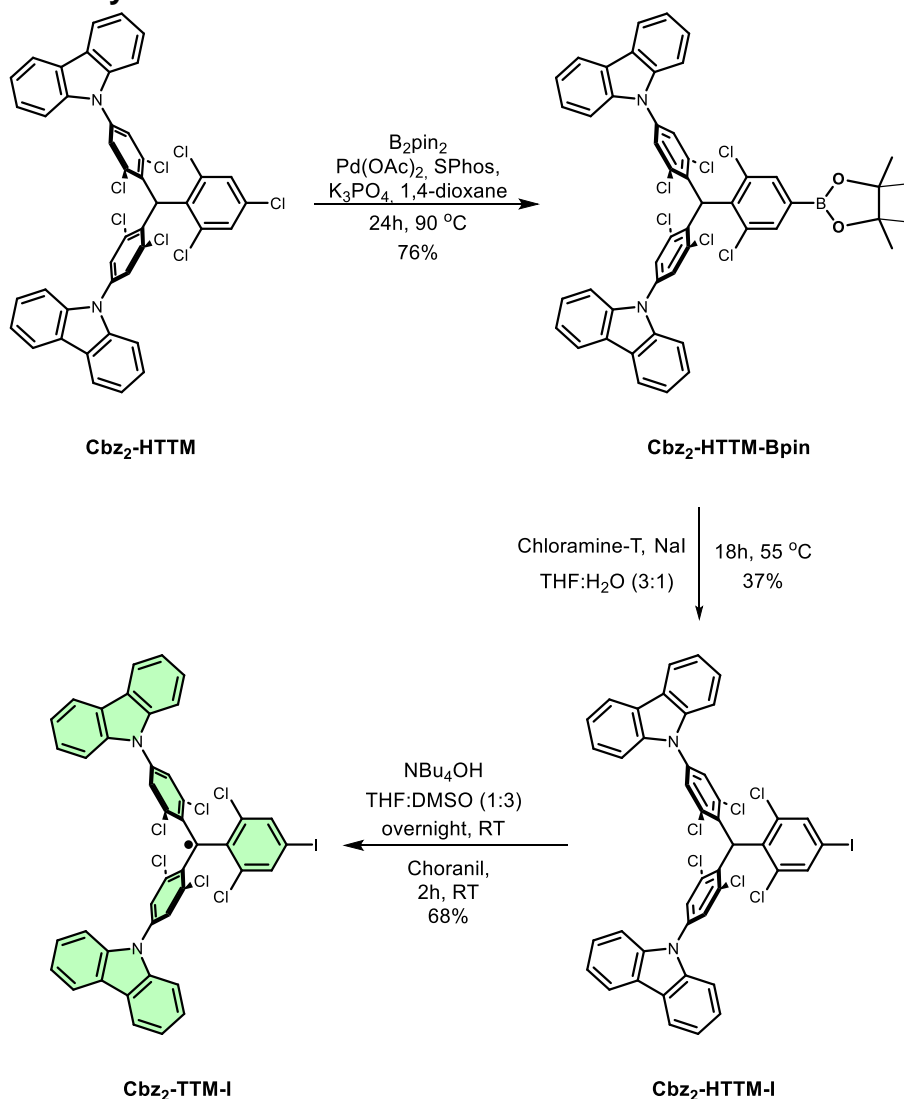
A mixture of **TTM** (3.00g, 1.81 mmol), carbazole (1.51 g, 9.0 mmol), anhydrous Cs₂CO₃ (0.94 g, 2.9 mmol), and DMF (20 mL) was stirred at 160°C for 2.5 h under argon atmosphere and in the dark. After the reaction mixture cooled to room temperature, the resulting mixture was poured into (1 M) hydrochloric acid solution, and the precipitate was filtered. The crude product was adsorbed in silica gel and purified by silica gel column chromatography using (petroleum ether:dichloromethane = 5:1 v/v), giving the desired compound **Cbz-HTTM** as a light brown solid (1.19 g, 32%) and **Cbz₂-HTTM** as a dark green solid (0.62 g, 14%). The characterization data is in good agreement with the literature.²

¹H NMR (600 MHz, CDCl₃) δ 8.15 (d, *J* = 7.6 Hz, 4H), 7.69 (dd, *J* = 14.7, 2.3 Hz, 2H), 7.56 (dd, *J* = 14.7, 2.3 Hz, 2H), 7.50–7.46 (m, 9H), 7.36–7.33 (m, 5H), 7.05 (s, 1H).

¹³C {¹H} NMR (150 MHz, CDCl₃) δ 140.29, 140.28, 138.66, 138.64, 138.22, 138.16, 137.92, 137.86, 137.49, 134.41, 134.28, 133.99, 130.35, 128.73, 128.48, 128.41, 126.83, 126.78, 126.47, 123.93, 120.93, 120.66, 109.75, 50.25.

HR-MS (FTICR-MALDI, matrix: DCTB): *m/z* [M]⁺ calc. for C₄₃H₂₃Cl₇N₂: = 813.9651, found: 813.9628; δ*m/m* = 2.8 ppm.

2.2 Synthesis of Cbz₂-TTM-I



Scheme S2 Synthesis of **Cbz₂-TTM-I**

Synthesis of Cbz₂-HTTM-Bpin

Cbz₂-HTTM (0.5 g, 0.61 mmol), bis(pinacolato)diboron (1.56 g, 6.13 mmol), Pd(OAc)₂ (6.88 mg, 0.03 mmol), SPhos (25.16 mg, 0.061 mmol) and K₃PO₄ (0.390 g, 1.84 mmol) were added into a glass pressure vessel was subjected to three vacuum/Ar gas refill cycles. Anhydrous 1,4-dioxane (20 mL) was added and degassed for 10 min with argon. The mixture was heated at 90 °C in an oil bath for 24 h. After cooling to RT, the mixture was diluted with dichloromethane, extracted with brine and water (3 × 200 mL) and the organic phase was dried over anhydrous MgSO₄. The solvent was removed under vacuum and the crude product was purified by precipitation from dichloromethane and methanol. The solids were collected by centrifuging and the solvent was removed by pipetting and the solids were dried in a vacuum. The target compound was collected as a pale-yellow solid (0.42 g, 76%).

¹H NMR (400 MHz, CD₂Cl₂) δ 8.16 (d, *J* = 7.6 Hz, 4H), 7.82 (d, *J* = 10.5 Hz, 1H), 7.71 – 7.66 (m, 3H), 7.58 (dd, *J* = 15.5, 2.3 Hz, 2H), 7.52 – 7.45 (m, 8H), 7.33 (t, *J* = 7.3 Hz, 4H), 7.12 (s, 1H), 1.36 (s, 12H).

^{13}C $\{^1\text{H}\}$ NMR (100 MHz, CD_2Cl_2) δ 140.63, 140.58, 138.98, 138.31, 138.26, 138.15, 137.72, 137.09, 136.54, 135.03, 135.00, 134.66, 128.75, 128.66, 127.08, 127.04, 126.70, 124.10, 121.14, 120.79, 120.70, 110.09, 85.03, 51.37, 25.12, 25.04.

HR-MS (FTICR-MALDI, matrix: DCTB): m/z $[\text{M}]^+$ calc. for $\text{C}_{49}\text{H}_{35}\text{BCl}_6\text{N}_2\text{O}_2$: = 906.0908, found: 906.0993; $\delta m/m$ = 9.3 ppm.

Synthesis of **Cbz₂-HTTM-I**

Compound **Cbz₂-HTTM-Bpin** (200 mg, 0.22 mmol) is suspended in 16 mL of a 1/3 water/THF mixture. Chloramine-T (931 mg, 3.31 mmol) and sodium iodide (495 mg, 3.31 mmol) were added to the reaction, and the vessel was sealed and heated at 55 °C for 12 hours without light. After cooling the reaction to room temperature, 10 mL of a saturated solution of sodium sulfite is added to the reaction. The resulting crude product was extracted several times with dichloromethane. The organic phase was collected and dried over anhydrous magnesium sulfate and the solvent was removed under vacuum. The crude product was adsorbed in silica gel and purified by silica gel column chromatography using pure petroleum ether as the eluent, giving the desired **Cbz₂-HTTM-I** as an off-white solid (74 mg, 37%).

^1H NMR (400 MHz, CD_2Cl_2) δ 8.16 (d, J = 7.8 Hz, 4H), 7.83 – 7.79 (m, 1H), 7.71 – 7.67 (m, 3H), 7.55 (dd, J = 9.4, 2.4 Hz, 2H), 7.52 – 7.44 (m, 8H), 7.33 (t, J = 7.3 Hz, 4H), 7.03 (s, 1H).

^{13}C $\{^1\text{H}\}$ NMR (100 MHz, CD_2Cl_2) δ 140.59, 139.10, 138.93, 138.87, 138.56, 138.44, 138.20, 138.12, 137.73, 137.38, 135.95, 134.55, 134.51, 128.79, 128.68, 127.09, 126.71, 124.15, 121.14, 120.81, 110.06, 92.22, 51.00.

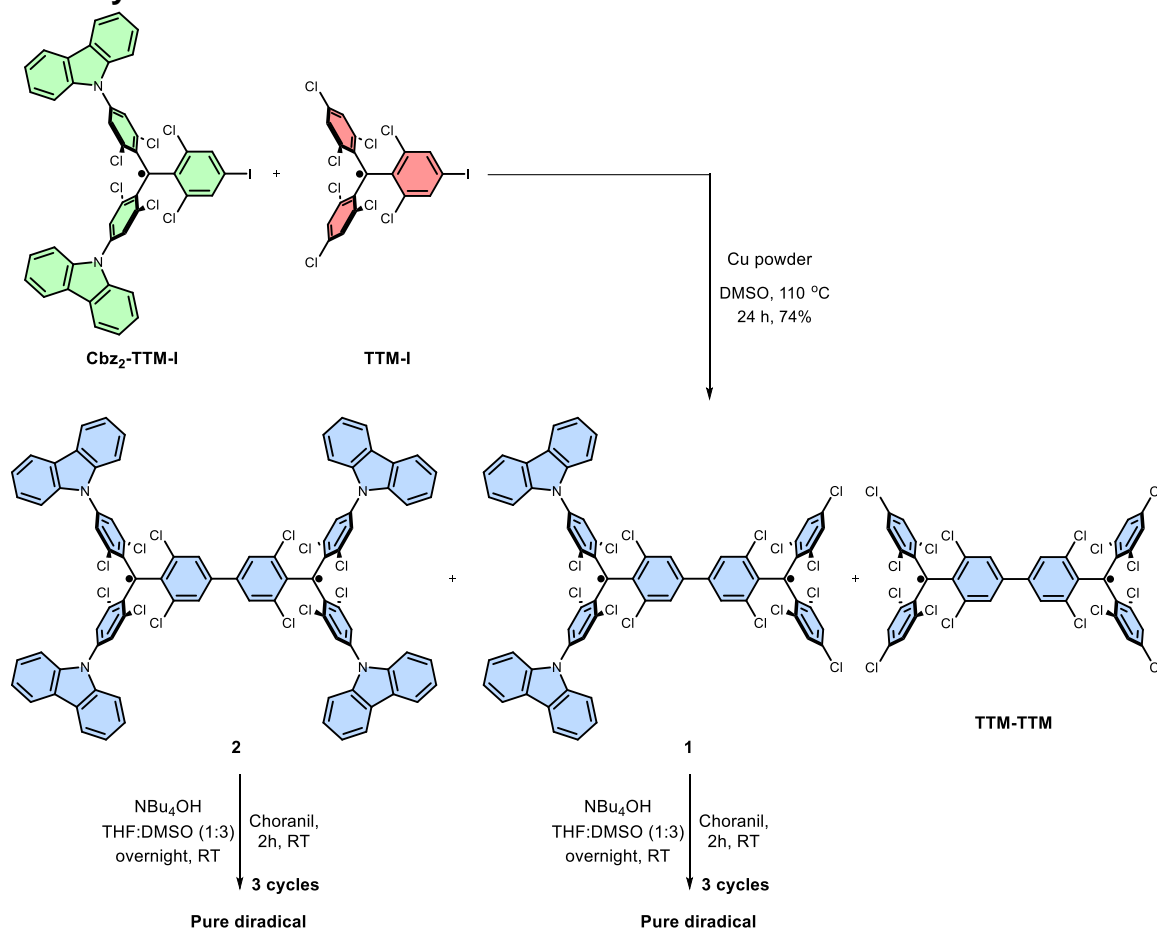
HR-MS (FTICR-MALDI, matrix: DCTB): m/z $[\text{M}]^+$ calc. for $\text{C}_{43}\text{H}_{23}\text{Cl}_6\text{N}_2$: = 905.9011, found: 905.9002; $\delta m/m$ = 1.0 ppm.

Synthesis of **Cbz₂-TTM-I**

Under argon atmosphere and in the dark, a tetrabutylammonium hydroxide 40 wt.% (1.5 M) solution in water (0.52 mL, 0.82 mmol) was added to a solution of **Cbz₂-HTTM-I** (74 mg, 0.082 mmol) in degassed DMSO/THF (3/1) (10 mL). After the mixture was stirred for overnight at room temperature, tetrachloro-*p*-benzoquinone (0.2 g, 0.82 mmol) was added to the reaction mixture and allowed to react another 2 h. After the reaction was finished, the THF was removed under vacuum. The resulting crude product was extracted several times with dichloromethane. The organic phase was collected and dried over anhydrous magnesium sulfate and the solvent was removed under vacuum. The crude product was adsorbed in silica gel and purified by silica gel column chromatography using petroleum ether/dichloromethane (5/1) as the eluent, giving the desired **Cbz₂-TTM-I** radical as a dark green powder (50.2 mg, 68%).

HR-MS (FTICR-MALDI, matrix: DCTB): m/z $[\text{M}]^+$ calc. for $\text{C}_{43}\text{H}_{22}\text{Cl}_6\text{N}_2$: = 904.8929, found: 904.8919; $\delta m/m$ = 1.1 ppm.

2.3 Synthesis of 1 and 2



Scheme S3 Synthesis of **TTM-TTM**, **1** and **2**.

Procedure

TTM-I (35.6 mg, 0.055 mmol), Cbz₂-TTM-I (50 mg, 0.055 mmol) and Cu powder (Aldrich, powder, 99.5% trace metals basis, 70.1 mg, 1.10 mmol) were added to degassed, anhydrous DMSO (3 mL) in a Schlenk flask under argon atmosphere. The reaction vessel was covered with aluminium foil to exclude ambient light and heated to 110 °C with vigorous stirring for 24 h. The reaction was allowed to cool to room temperature. The mixture was poured into water and extracted with DCM (15 mL x 3). The organic phase was washed with EDTA solution and then dried over MgSO₄. After filtration and removal of the solvent, the crude product was purified by a silica gel column using a dichloromethane and petroleum ether mixture (v/v, 1/5 to 1/1) as the mobile phase. The blue spots on the TLC plate with an *R_f* value of 0.8 was **TTM-TTM** (13.7 mg, 24% yield), 0.6 was Cbz₂-TTM-TTM (**1**) (23.6 mg, 33% yield), and 0.4 was Cbz₂-TTM-TTM-Cbz₂ (**2**) (14.6 mg, 17% yield) (dichloromethane:petroleum ether (3:7)) (see figure S1).

Cbz₂-TTM-TTM (**1**)

¹H NMR (400 MHz, CD₂Cl₂, 298 K): by dissolving 1 mg of compound in 0.5 mL of CD₂Cl₂, showing **1** is NMR silent (Figure S8.5a).

HR-MS (FTICR-MALDI, matrix: DCTB): *m/z* [M]⁺ calc. for C₆₂H₂₈Cl₁₄N₂: = 1295.7818, found: 1295.7823; $\delta m/m$ = 0.38 ppm.

Cbz₂-TTM-TTM-Cbz₂ (2)

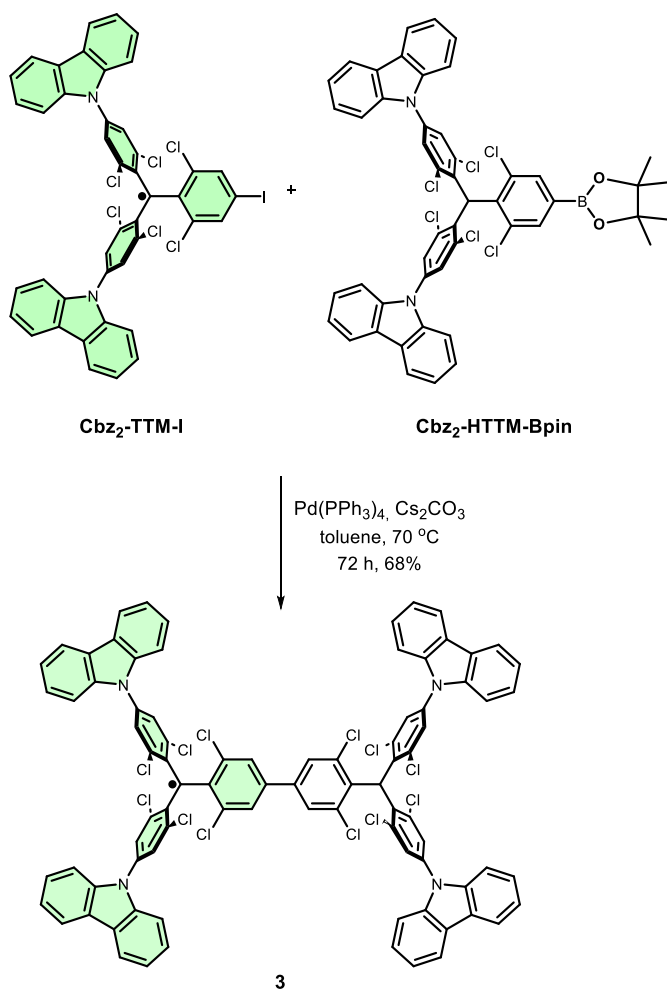
¹H NMR (400 MHz, CD₂Cl₂, 298 K): by dissolving 1 mg of compound in 0.5 mL of CD₂Cl₂, showing **2** is NMR silent (Figure S8.6a).

HR-MS (FTICR-MALDI, matrix: DCTB): m/z [M]⁺ calc. for C₈₆H₄₄Cl₁₂N₄: = 1557.9770, found: 1557.9796; δm/m = 1.67 ppm.

Purification of 1 and 2 by base/oxidation cycles

Under an argon atmosphere and in the dark, a 40 wt.% (1.5 M) solution of tetrabutylammonium hydroxide (20 equiv.) in water was added to a solution of the crude diradical in degassed DMSO/THF (3/1) (10 mL). The mixture was stirred overnight at room temperature, after which tetrachloro-*p*-benzoquinone (20 equiv.) was added, and the reaction was allowed to proceed for an additional 2 hours. Upon completion, the THF was removed under vacuum, and the crude product was extracted multiple times with dichloromethane. The organic phase was collected, dried over anhydrous magnesium sulfate, and the solvent was removed under vacuum. The crude product underwent for 3 (for **1**) and 5 (for **2**) cycles base/oxidation treatment, repeating the same procedure as described earlier. Finally, the crude diradical was purified by silica gel column chromatography (short plug) using petroleum ether/dichloromethane (1/1) as the eluent to yield the desired diradical. The product was then further purified by recycling gel permeation chromatography (GPC) to achieve high purity.

2.4 Synthesis of Cbz₂-TTM-HTTM-Cbz₂ (3)



Scheme S4 Synthesis of 3.

Synthesis of 3

Cbz₂-TTM-I (45 mg, 0.049 mmol), **Cbz₂-HTTM-BPin** (45 mg, 0.049 mmol), Cs₂CO₃ (97 mg, 0.297 mmol), and Pd(PPh₃)₄ (4 mg, 0.003 mmol) were added to degassed toluene (7 mL) in a Schlenk flask under argon atmosphere. The reaction vessel was covered with aluminium foil to exclude ambient light and heated to 70 °C while stirring for 72 h. The reaction was allowed to cool to room temperature. The solvent was removed, and the crude product was purified by a silica gel column using a dichloromethane and hexane mixture (v/v, 1/1) as the mobile phase. The solvent was removed under reduced pressure, yielding an dark green powder (52.6 mg, 68% yield).

¹H NMR (400 MHz, CD₂Cl₂, 298 K): by dissolving 1 mg of a compound in 0.5 mL of CD₂Cl₂, broad signals were found in the ¹H NMR spectrum due to the paramagnetic character. (Figure S8.7a)

HR-MS (FTICR-MALDI, matrix: DCTB): m/z [M]⁺ calc. for C₈₆H₄₅Cl₁₂N₄: = 1558.9848, found: 1558.9868; δm/m = 1.28 ppm.

3. Purification and HPLC-MS analysis

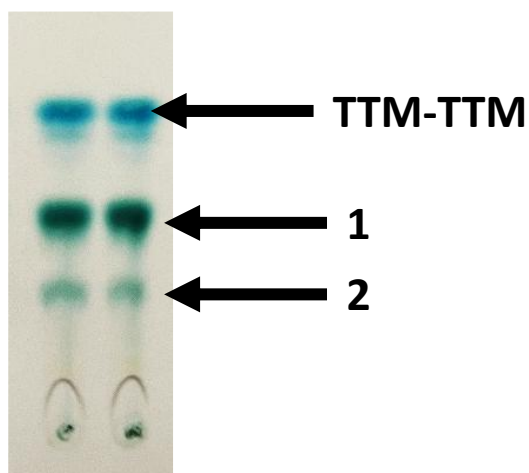


Figure S1 Daylight photograph of the TLC plate developed with a dichloromethane:petroleum ether (3:7) solvent mixture, showing the reaction mixture (Scheme S3).

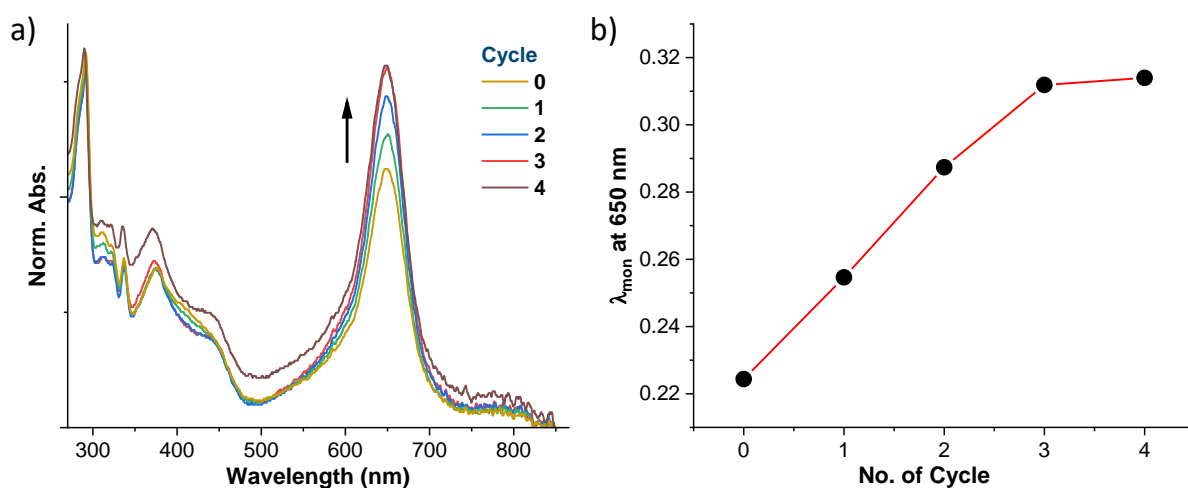


Figure S2 Normalized UV-Visible spectrum of **2** with cycles of base treatment followed by oxidation; solvent: dichloromethane.

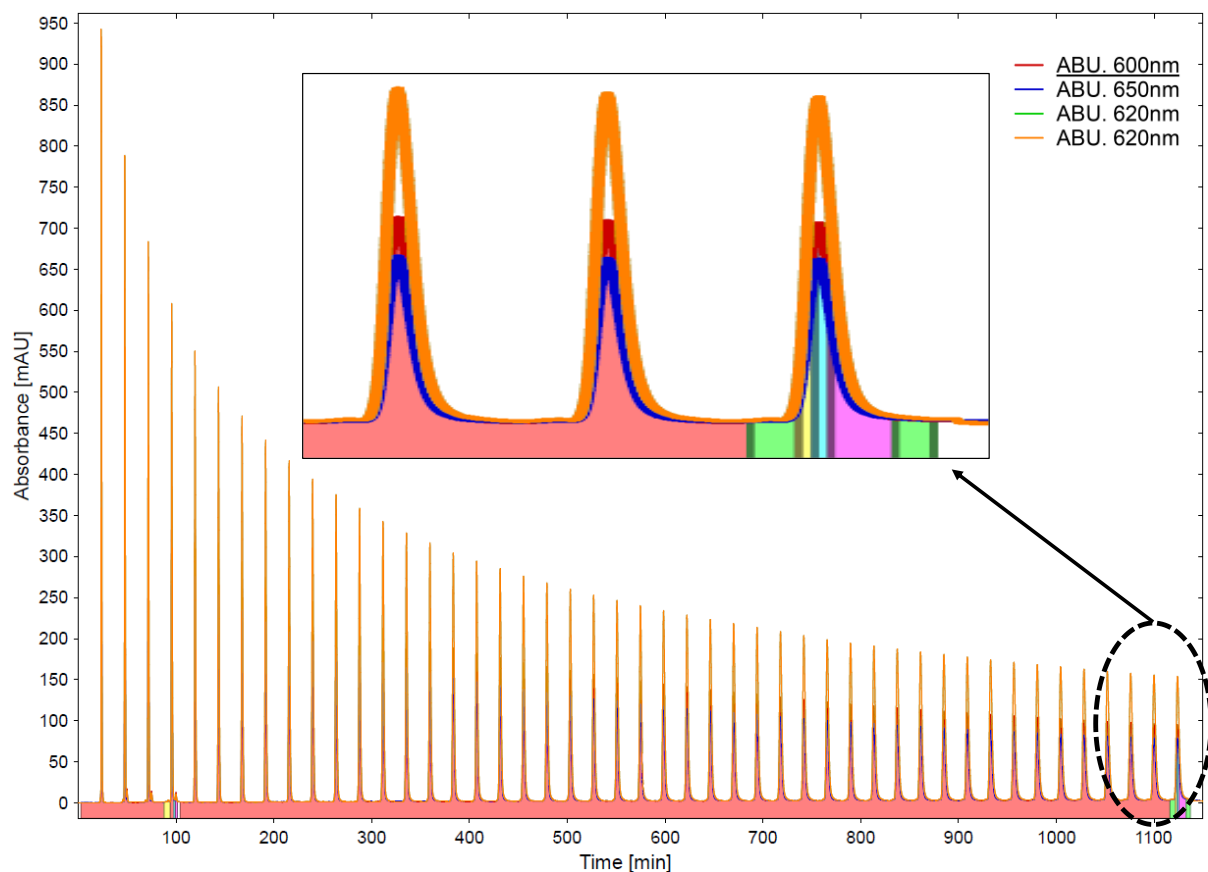


Figure S3 Recycling GPC showing various cycles of purifications of **1**. Eluent: Dichloromethane Flow rate: 10 mL/min Detector: UV-Vis 4ch LA @ 600-650 nm Sample: 1 mg/mL; Injection Volume: 8.0 mL.

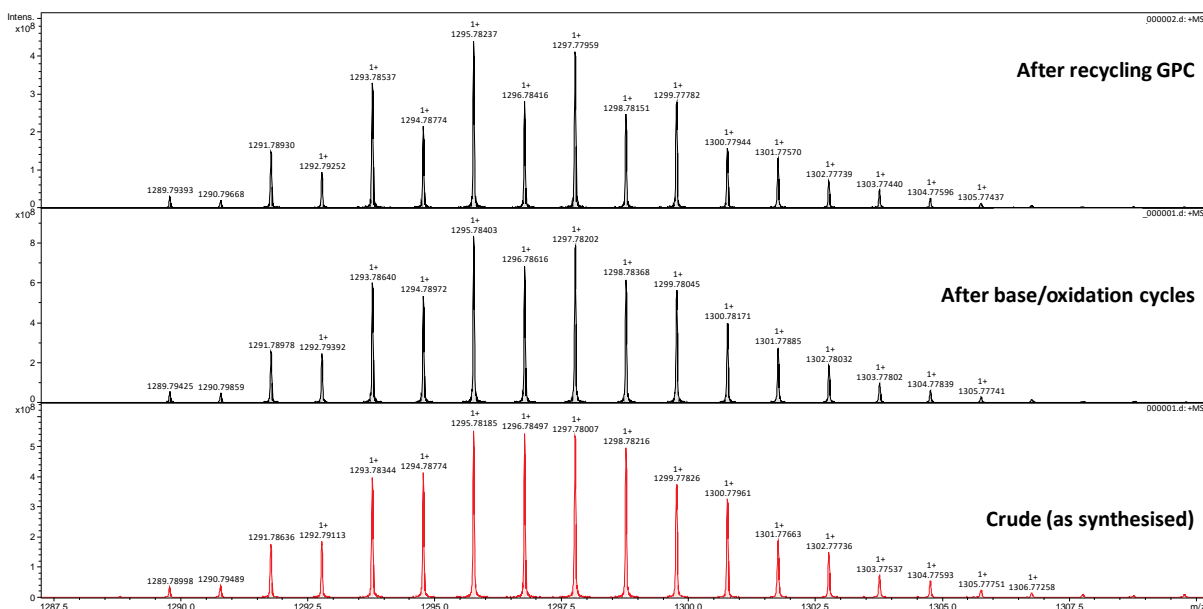


Figure S4 MALDI-MS analysis of crude diradical **1** compare with purification after base/oxidation treatment and recycling GPC showing significant deviations to the isotopic patterns.

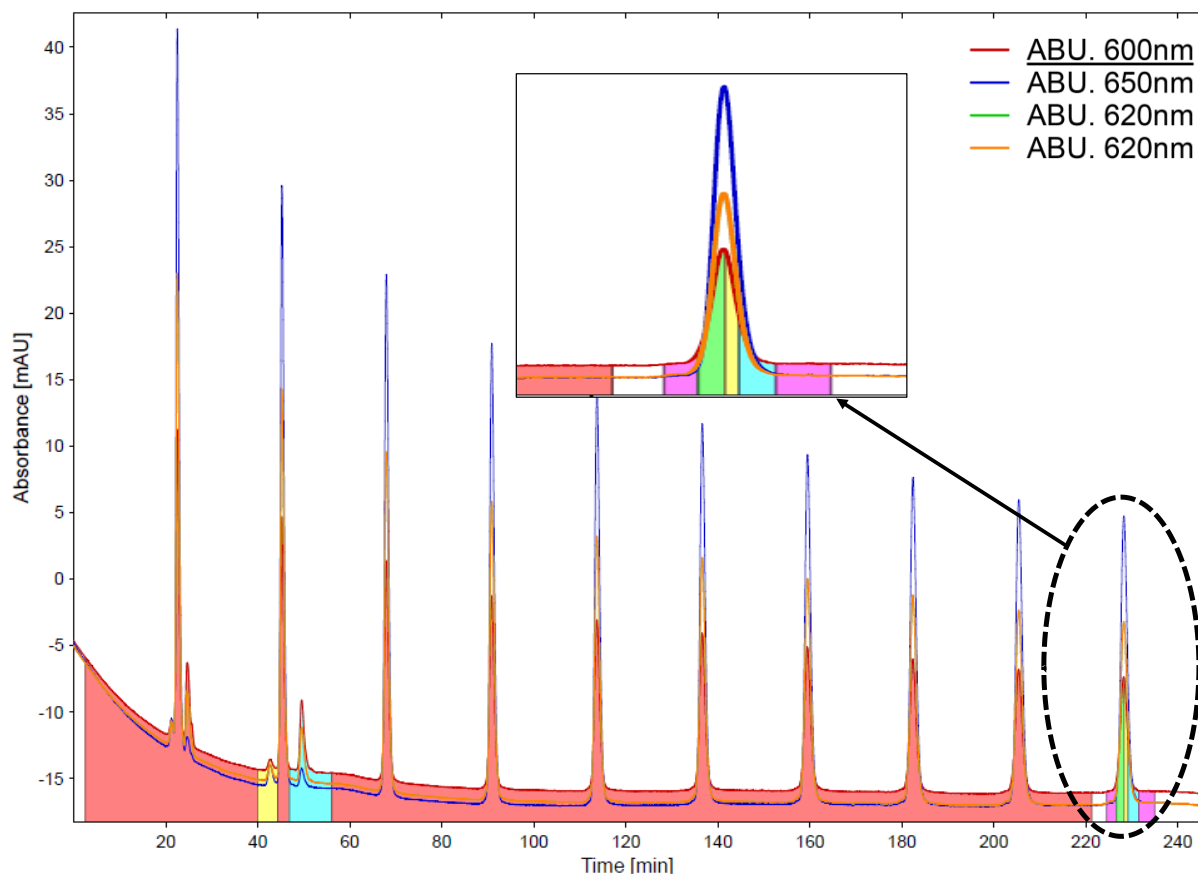


Figure S5 Recycling GPC showing various cycles of purifications of **2**. Eluent: Dichloromethane Flow rate: 10 mL/min Detector: UV-Vis 4ch LA @ 600-650 nm Sample: 0.25 mg/mL; Injection Volume: 8.0 mL.

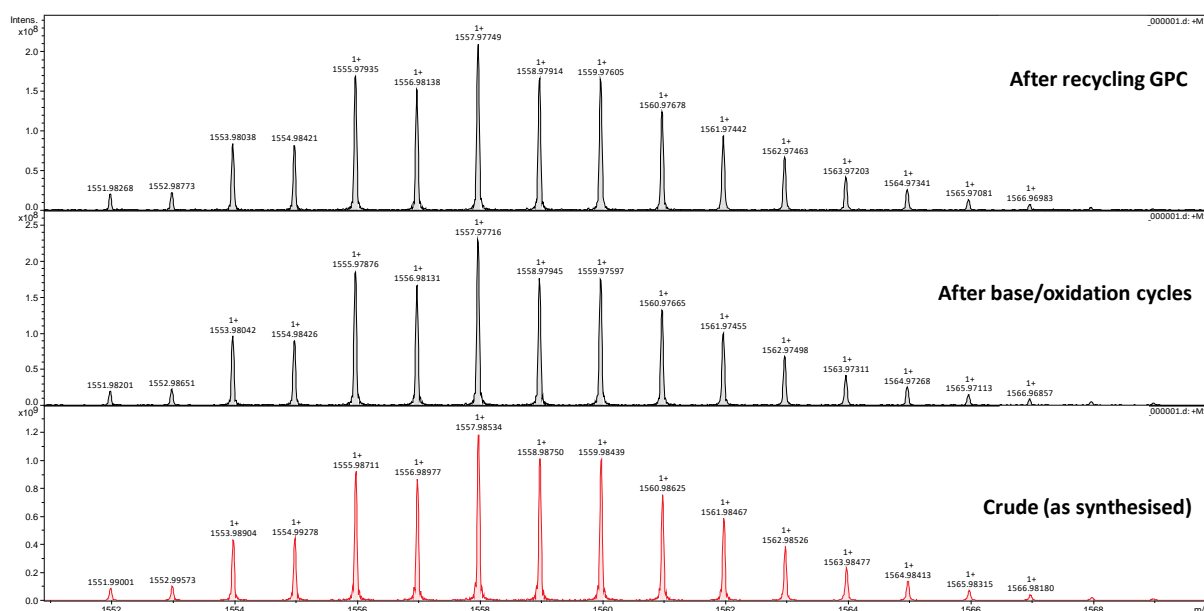


Figure S6 MALDI-MS analysis crude diradical **2** compare with purification after base/oxidation treatment and recycling GPC showing significant deviations to the isotopic patterns.

Further, HPLC-MS analyses were carried out to demonstrate the high purity of samples. The compounds were dissolved in toluene (HPLC grade) and filtered. We chose toluene and a

mixture of toluene and *n*-hexane (v/v, 7:3) as the mobile phases and selected an analytical Buckyprep M column as stationary phase with flow rate 0.5 mL/min. As shown in Figures S7-S8, all PDA and 2D-mapping spectra of **diradicals** displayed single-component traces, confirming their high chemical purity.

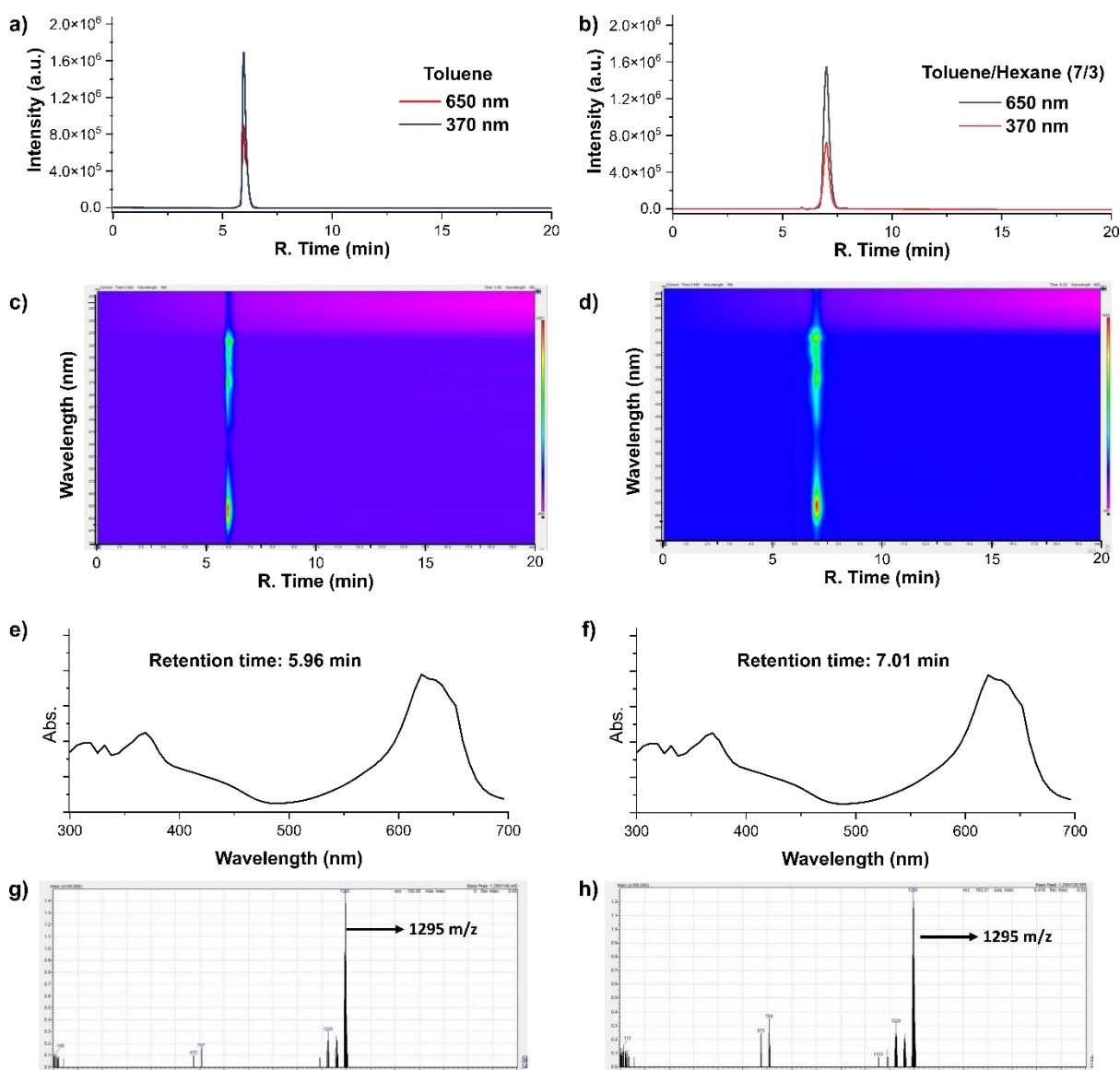


Figure S7 HPLC-MS characterization of **1** with toluene (a, c, e, and g) and mixture of toluene and hexane (b, d, f, and h) as mobile phases. HPLC chromatogram (a and b) and photodiode array mapping (c and d) of **1**. The UV-Vis absorption spectra and mass spectra of sample at 5.96 min (e and g) in toluene and 7.01 min (f and h) in mixture of toluene and hexane.

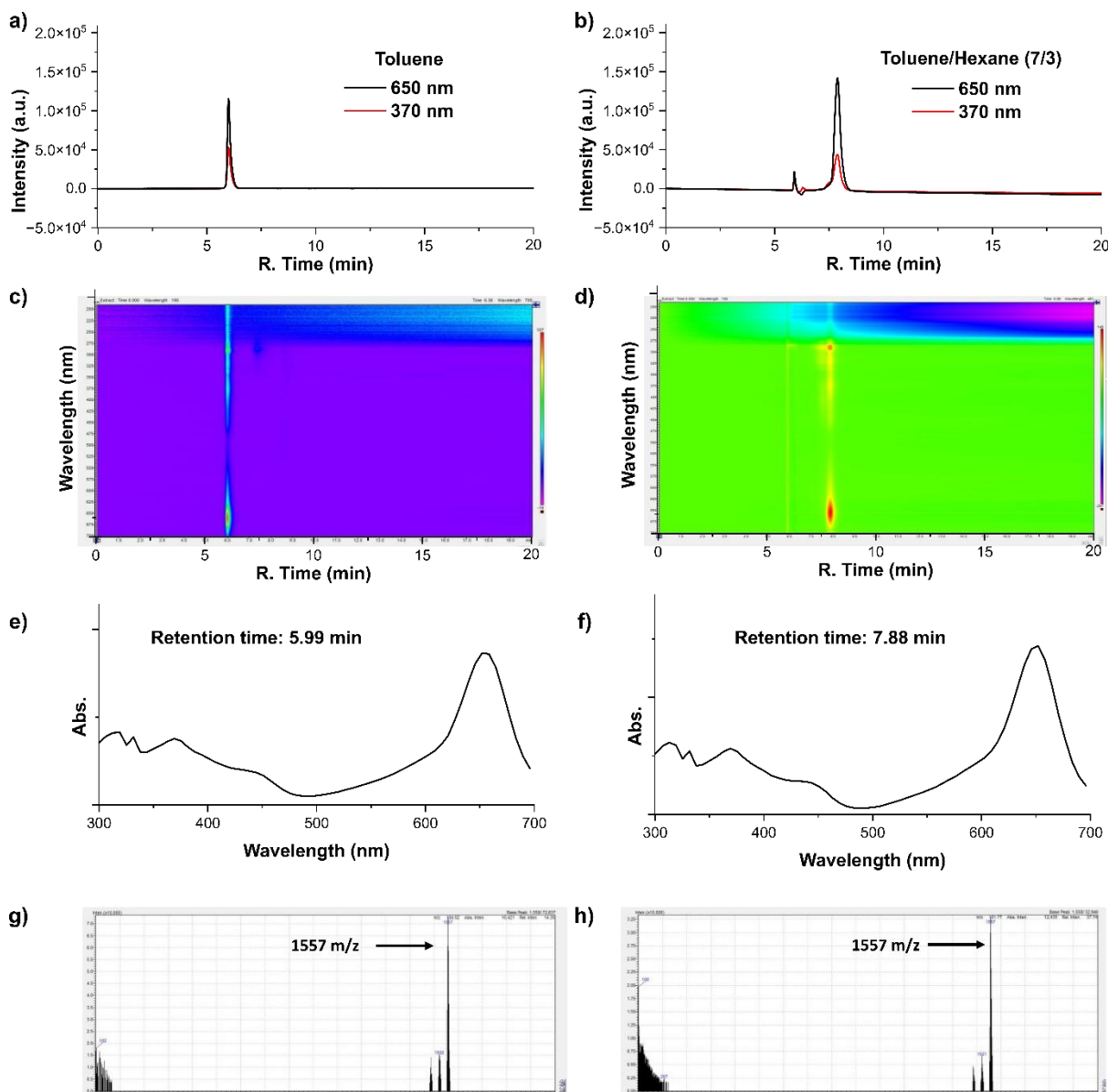


Figure S8 HPLC-MS characterization of **2** with toluene (a, c, e, and g) and mixture of toluene and hexane (b, d, f, and h) as mobile phases. HPLC chromatogram (a and b) and photodiode array mapping (c and d) of **2**. The UV-Vis absorption spectra and mass spectra of sample at 5.99 min (e and g) in toluene and 7.88 min (f and h) in mixture of toluene and hexane. (Due to the poor solubility of compound **2** in the toluene/hexane mixture, a residue was observed on the column at a retention time of 5.99 min).

4. Cyclic voltammetry measurements

A 1 mg/mL in concentration of each compound in dry dichloromethane solvent was prepared for cyclic voltammetry measurements. The supporting electrolyte used was 0.1 M *n*-butylammonium hexafluorophosphate ($n\text{Bu}_4\text{N})(\text{PF}_6)$, and the experiments were conducted under argon atmosphere at 25°C. A glassy carbon electrode served as the working electrode, a platinum wire as the counter electrode, and the reference electrode was Ag/Ag⁺. All CV potentials were referenced to the ferrocene/ferrocenium (Fc/Fc⁺) couple.

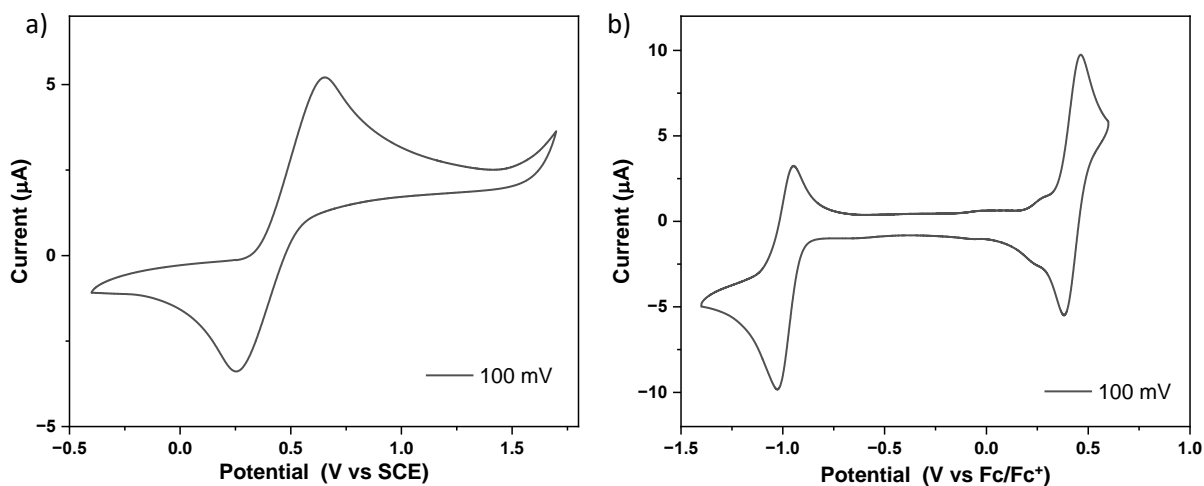


Figure S9 Cyclic voltammogram of a) Reference Fc and Cbz₂-TTM-I at a scan rate of 100 mV/s.

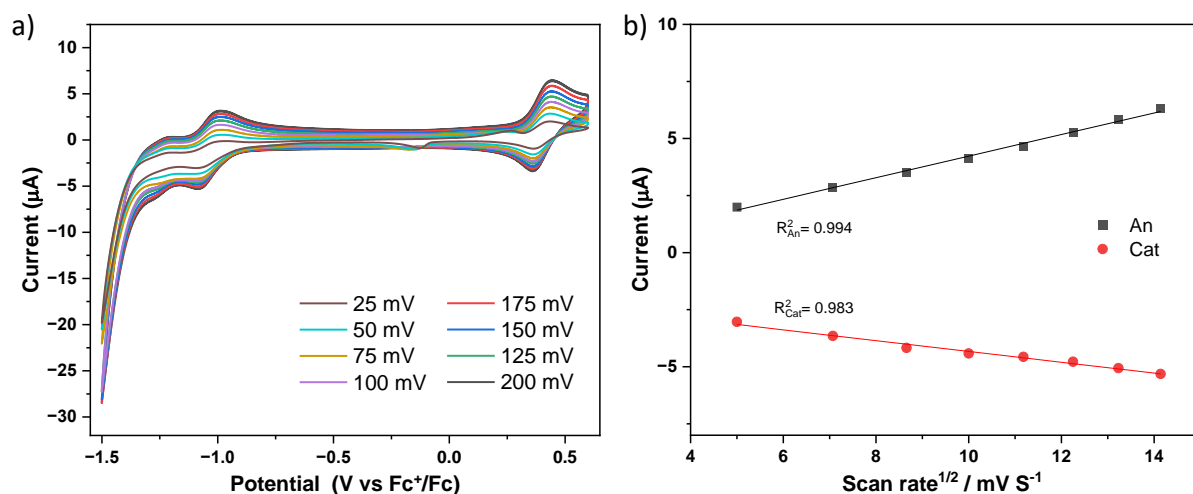


Figure S10 a) Cyclic voltammograms at different scan rates (25 - 200 mV/s) and b) linear dependence between peak anodic current and scan rate^{1/2} of **3**.

Cyclic voltammetry (CV) clearly shows that diradical **1** exhibits sharp, reversible two-electron reduction and oxidation peaks, similar to its parent compound TTM-TTM. In contrast, diradical **2** does not display well-defined CV signals, primarily due to its poor solubility in the electrolyte medium. This limited solubility hampers efficient diffusion to the electrode surface, resulting in weaker and broadened electrochemical responses. Both diradicals contain carbazole units, which are known to undergo electropolymerization at the 3/6-positions during oxidation.⁹ The onset potential for this process is highly dependent on the electronic nature of the substituents.¹⁰ In the case of diradical **1**, the first two oxidation events associated with the radical centers occur before the onset of electropolymerization, allowing clear observation of the redox processes. In contrast, diradical **2** contains four electron-donating carbazole groups, making it significantly more electron-rich than diradical **1**. As a result, diradical **2**

undergoes electropolymerization at a lower potential, which contributes to its electrochemical instability and obscures its intrinsic redox behavior.

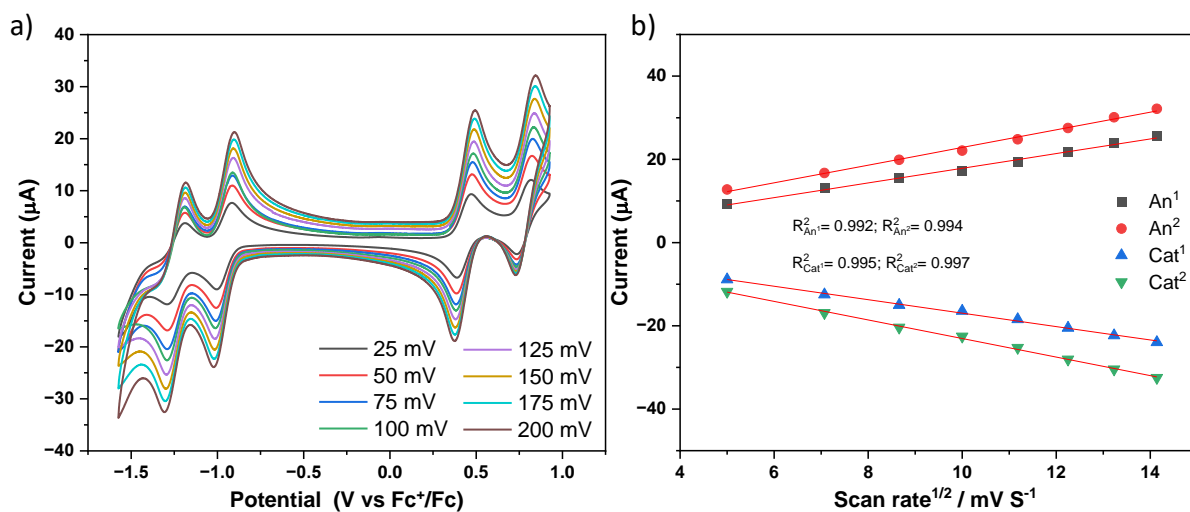


Figure S11 a) Cyclic voltammograms at different scan rates (25 - 200 mV/s) and b) linear dependence between peak anodic current and scan rate^{1/2} of **1**.

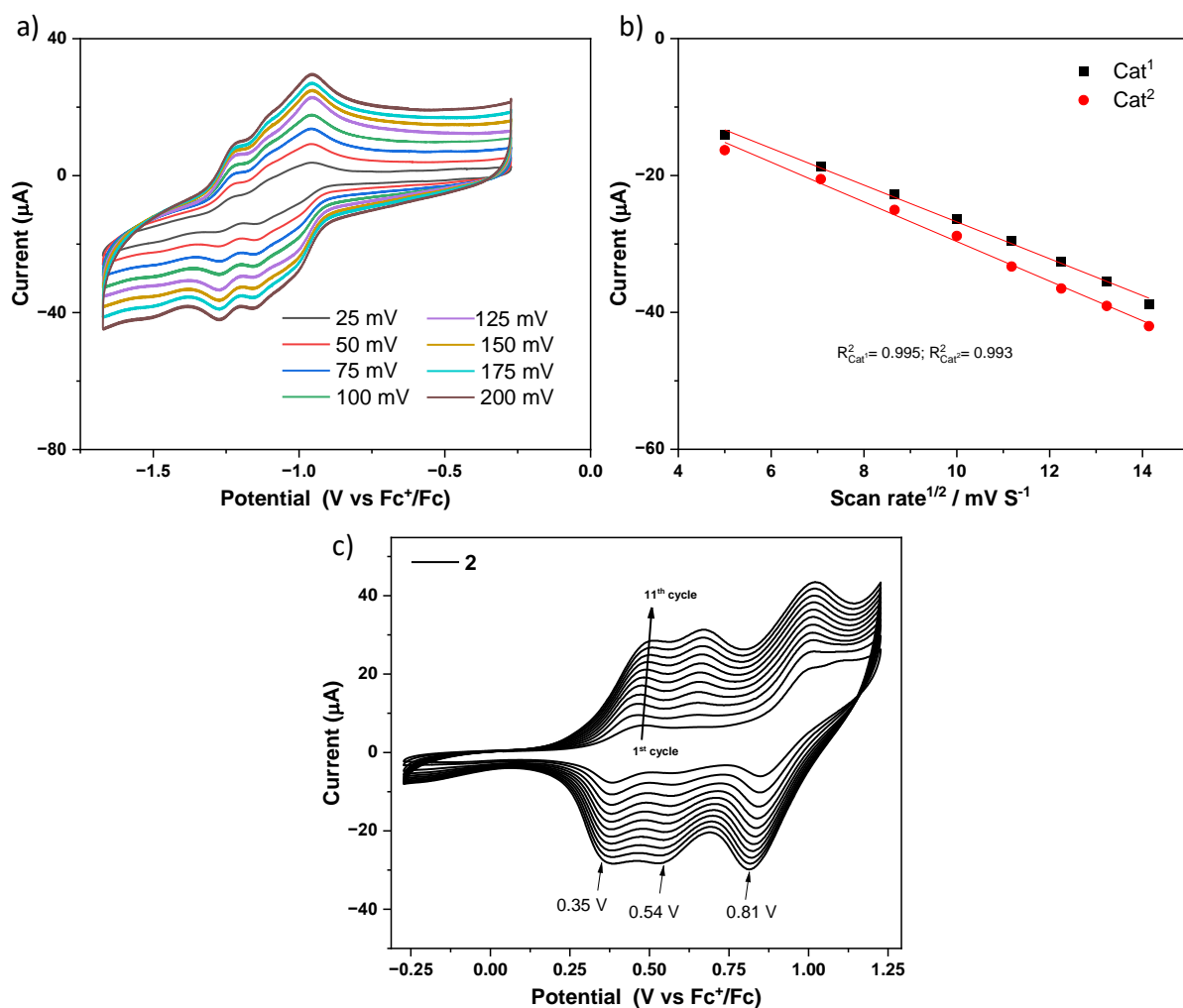


Figure S12 a) Cyclic voltammograms at different scan rates (25 - 200 mV/s) and b) linear dependence between peak anodic current and scan rate^{1/2} of **2** and c) Repetitive cyclic voltammograms of **2** at 100 mV/s (11 cycles).

5. Optical properties

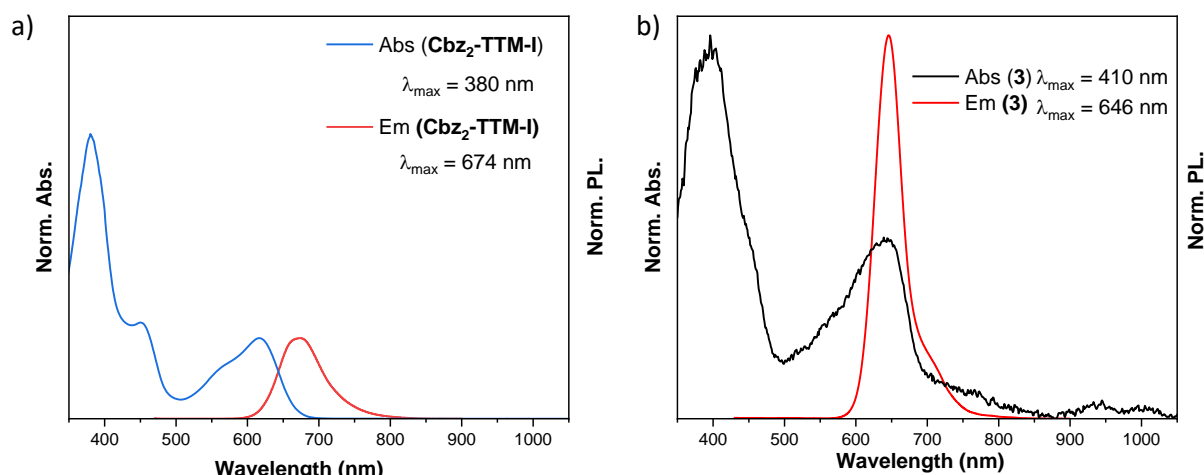


Figure S13 Normalized UV-Vis absorption and emission of a) Cbz₂-TTM-I and b) **3** in cyclohexane.

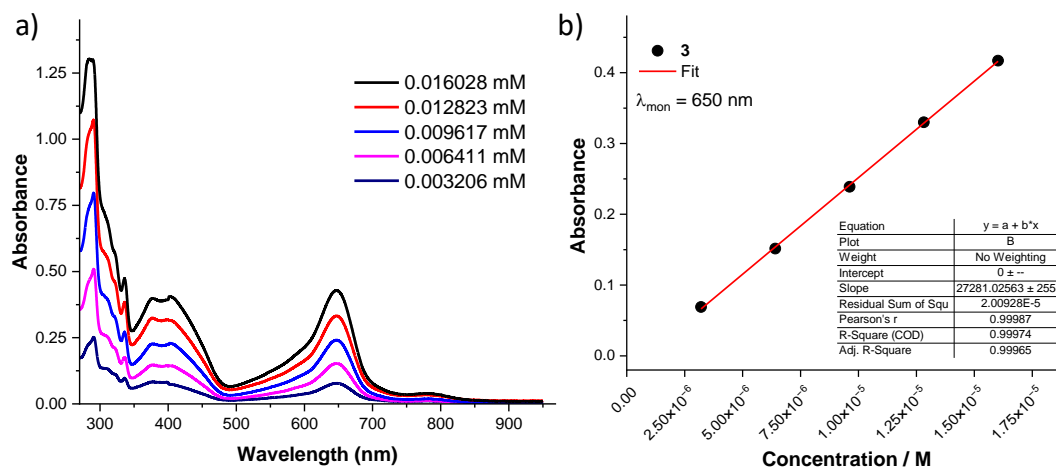


Figure S14 a) UV-Vis absorption spectra of **3** in dichloromethane with different concentrations. b) Linear fitting of absorption at 650 nm.

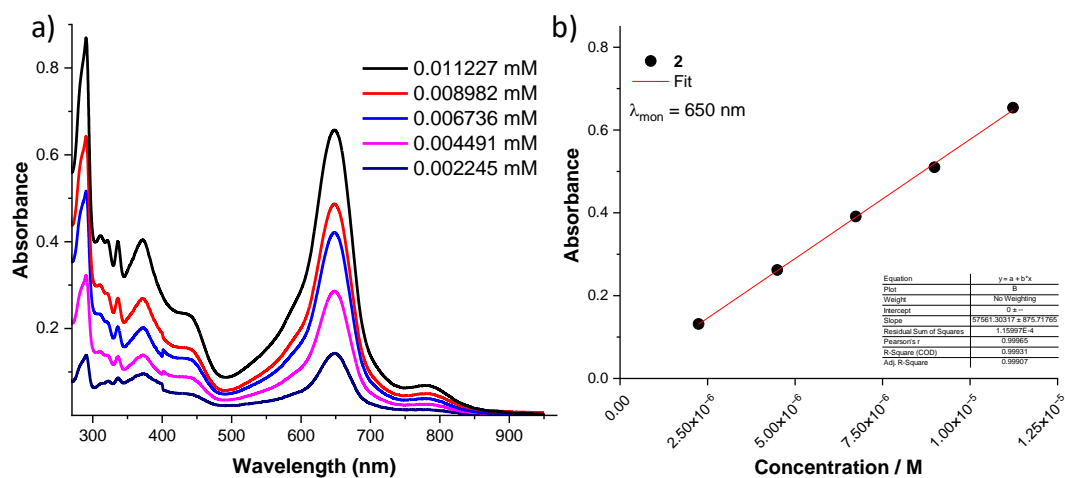


Figure S15 a) UV-Vis absorption spectra of **2** in dichloromethane with different concentrations. b) Linear fitting of absorption at 650 nm.

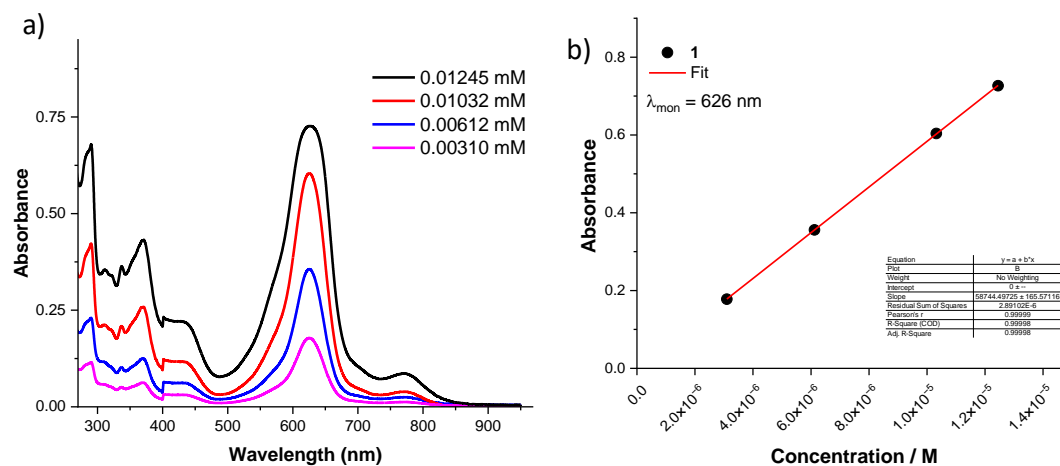


Figure S16 a) UV-Vis absorption spectra of **1** in dichloromethane with different concentrations. b) Linear fitting of absorption at 626 nm.

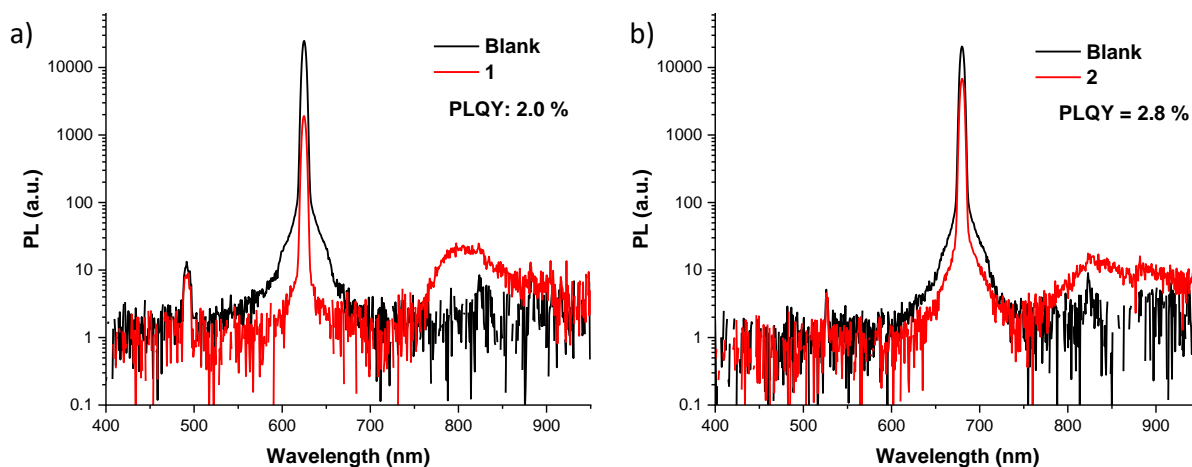


Figure S17 PLQYs of **1** and **2** in toluene.

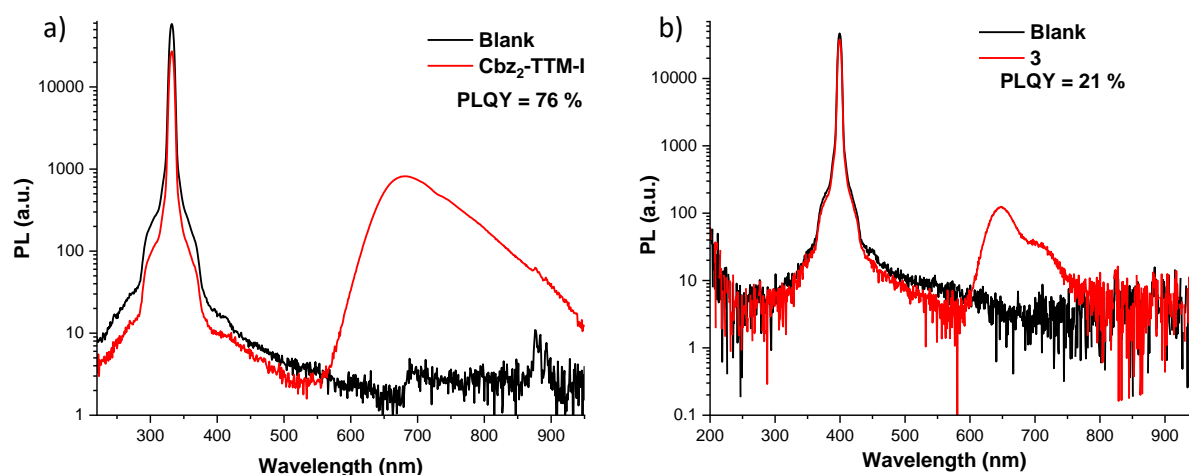


Figure S18 PLQYs of **Cbz₂-TTM-I** and **3** in cyclohexane.

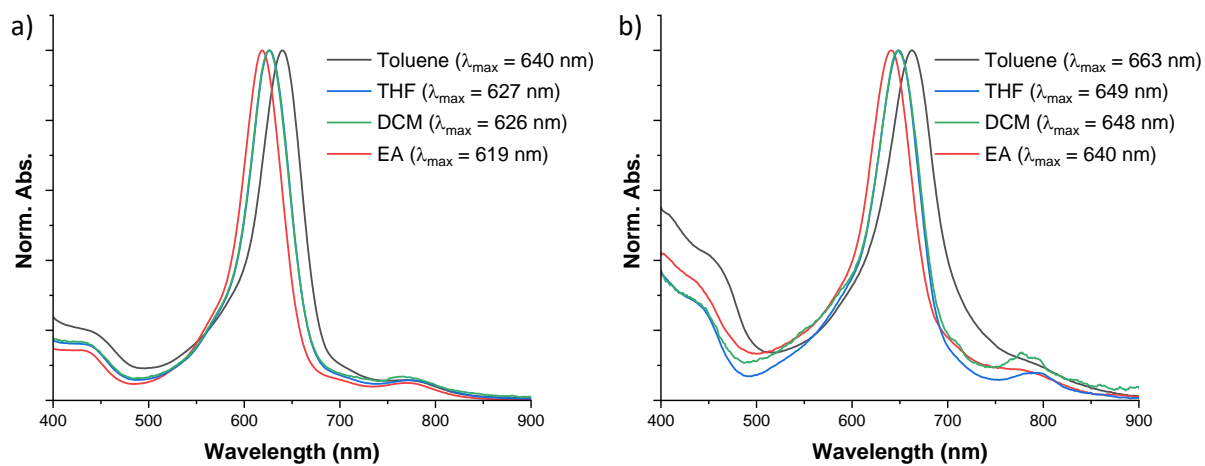


Figure S19 Normalized UV-Vis absorption of a) **1** and b) **2** in different Solvents.

6. DFT calculations

The theoretical calculations were performed with ORCA 5.0.3.³ The molecular geometry optimizations and the single-point calculations were carried out with the (unrestricted) B3LYP functional at the def2-TZVP level of theory in vacuum using dispersion correction with the Becke-Johnson damping scheme (D3BJ).⁴ Frequency analysis verified that all optimized structures do not contain any negative frequencies. TD-DFT calculation were performed at the B3LYP/def2-SVPD level of theory.^{4b,5} The coordinates of the geometry optimized structures can be downloaded from the Zenodo repository using the following link: doi.org/10.5281/zenodo.15363783

The singlet-triplet energy gap (ΔE_{ST}) was calculated with the Yamaguchi spin decontamination correction according to the following equation:⁶

$$\Delta E_{ST} = 2J = -\frac{2(E_T - E_{BS})}{\langle S^2 \rangle_T - \langle S^2 \rangle_{BS}}$$

Here, J corresponds to the intramolecular exchange interaction within the diradicals, E_T and E_{BS} represent the total energy of the calculated triplet and broken-symmetry state and $\langle S^2 \rangle_T$ and $\langle S^2 \rangle_{BS}$ correspond to the respective expectation value of the total spin squared operator. The diradical character y_0 was calculated from the occupation number of the highest occupied natural orbital (n_{HONO}) and of the lowest unoccupied natural orbital (n_{LUNO}) according to Yamaguchi:⁷

$$y_0 = 1 - \frac{2T_0}{1 + T_0^2}$$
$$T_0 = \frac{n_{HONO} - n_{LUNO}}{2}$$

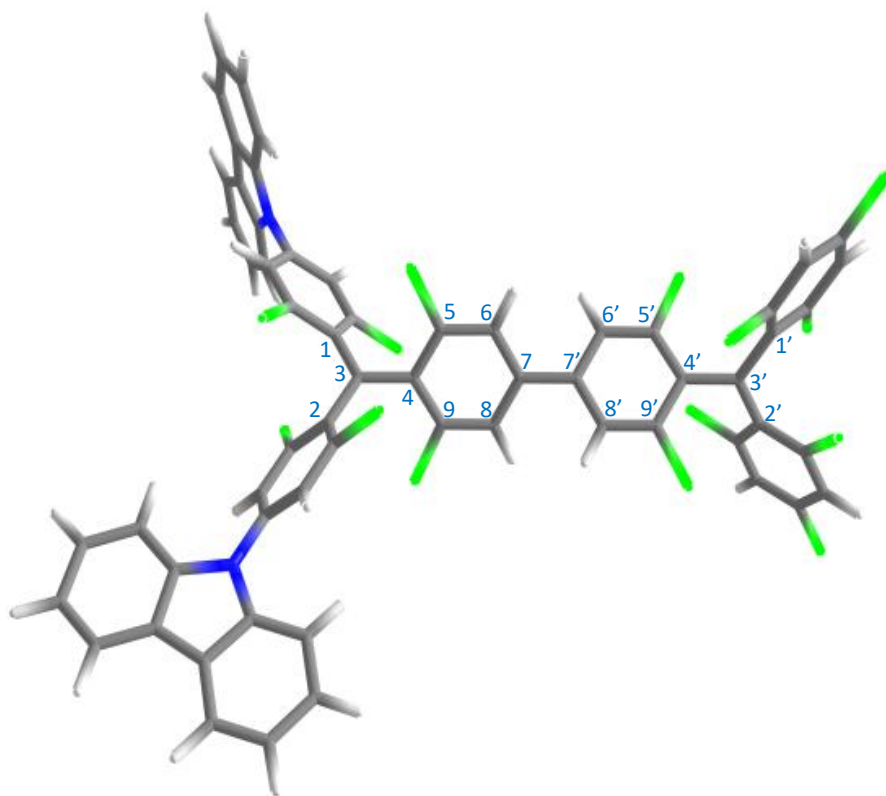


Figure S20 Geometry optimized structure of **1** ((U)B3LYP-D3/def2-TZVP).

Table S1 Selected bond lengths of the geometry optimized structure of **1** (UB3LYP-D3/def2-TZVP).

Key bonds / Å	OS singlet	triplet	closed shell
C1-C3	1.465	1.465	1.474
C2-C3	1.466	1.463	1.473
C3-C4	1.458	1.465	1.404
C4-C5	1.422	1.418	1.454
C4-C9	1.421	1.418	1.454
C5-C6	1.388	1.391	1.369
C9-C8	1.388	1.390	1.369
C6-C7	1.406	1.403	1.427
C8-C7	1.406	1.403	1.427
C7-C7'	1.475	1.480	1.427
C3-C3'	10.152	10.155	10.099
C4-C4'	7.235	7.225	7.293

Bond angles / °			
C1-C3-C2	119.5	119.9	116.5
C1-C3-C4	120.3	120.1	122.0
C2-C3-C4	120.1	119.9	121.5

Torsions / °			
C8-C7-C7'-C8'	28.38	32.82	4.57

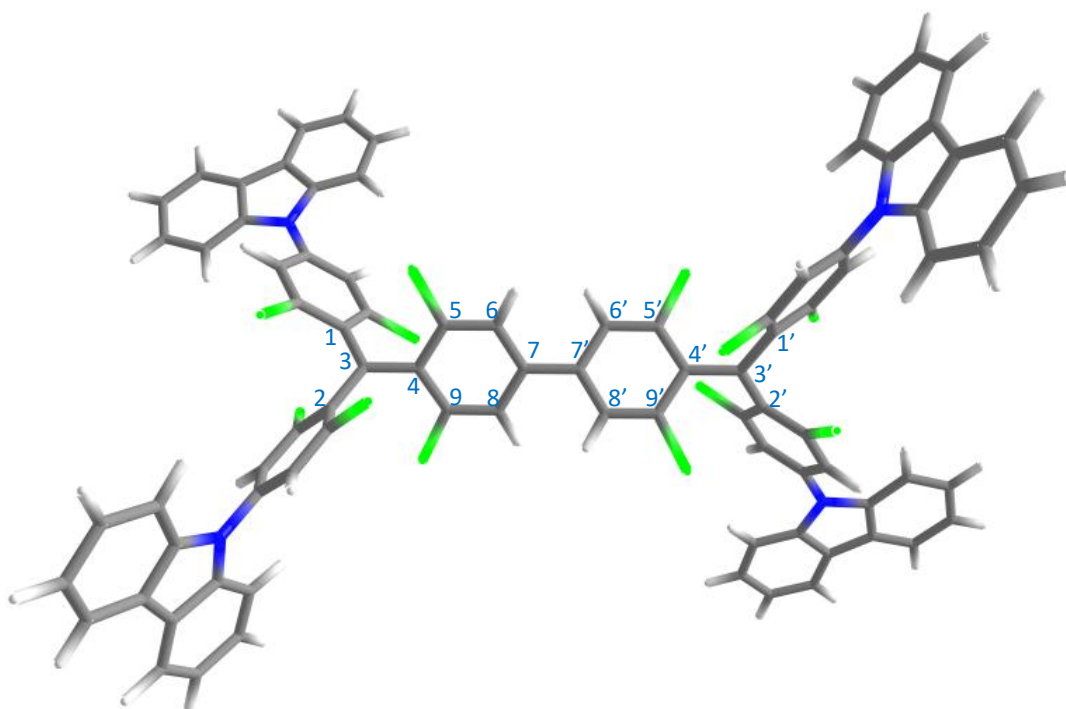


Figure S21 Geometry optimized structure of **2** (UB3LYP-D3/def2-TZVP).

Table S2 Selected bond lengths of the geometry optimized structure of **2** (UB3LYP-D3/def2-TZVP).

Key bonds / Å	OS singlet	triplet	closed-shell
C1-C3	1.464	1.463	1.473
C2-C3	1.466	1.465	1.475
C3-C4	1.458	1.466	1.404
C4-C5	1.421	1.417	1.454
C4-C9	1.421	1.417	1.454
C5-C6	1.388	1.390	1.369
C9-C8	1.388	1.390	1.369
C6-C7	1.406	1.404	1.427
C8-C7	1.406	1.404	1.426
C7-C7'	1.475	1.480	1.428
C3-C3'	10.155	10.158	10.101
C4-C4'	7.239	7.227	7.294
Bond angles / °			
C1-C3-C2	119.6	120.0	116.4
C1-C3-C4	120.2	120.0	121.7
C2-C3-C4	120.2	119.9	121.9
Torsions / °			
C8-C7-C7'-C8'	24.42	29.37	3.26

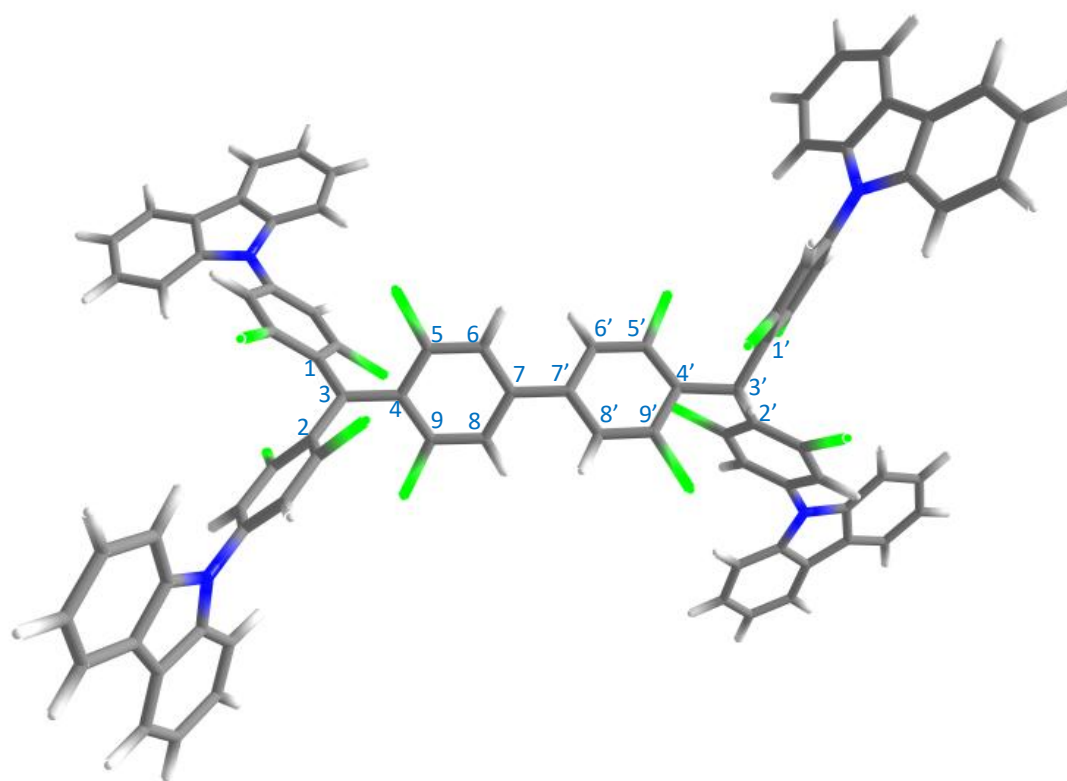


Figure S22 Calculated geometry structure of **3** (UB3LYP-D3/def2-TZVP).

Table S3 Selected bond lengths of the geometry optimized structure of **3** (UB3LYP-D3/def2-TZVP).

Key bonds / Å	doublet
C1-C3	1.463
C2-C3	1.465
C3-C4	1.463
C4-C5	1.419
C4-C9	1.419
C5-C6	1.390
C9-C8	1.390
C6-C7	1.404
C8-C7	1.404
C7-C7'	1.480
C3-C3'	10.211
C4-C4'	7.228
C1'-C3'	1.526
C2'-C3'	1.526
C3'-C4'	1.526

Bond angles / °	
C1-C3-C2	119.8
C1-C3-C4	120.1
C2-C3-C4	120.0
C1'-C3'-C2'	116.0
C1'-C3'-C4'	116.1
C2'-C3'-C4'	116.2
Torsions / °	
C8-C7-C7'-C8'	31.32

Table S4 Comparison of calculated values of geometry optimized structures of TTM-TTM, **1**, **2** and **3**

	TTM-TTM	1	2	3
E_D [Eh]	-	-	-	-9044.7708
E_T [Eh]	-8817.6446	-8930.8957	-9044.1443	-
E_{BS} [Eh]	-8817.6464	-8930.8967	-9044.1453	-
E_{CS} [Eh]	-8817.6360	-8930.8849	-9044.1337	-
ΔE_{ST} [kcal/mol]	-2.13	-1.22	-1.19	-
ΔE_{BS-CS} [kcal/mol]	-6.497	-7.413	-7.242	-
$\langle S^2 \rangle_T$	2.038	2.040	2.040	-
$\langle S^2 \rangle_{BS}$	1.0053	1.021	1.018	-
y_0	0.58	0.67	0.65	-

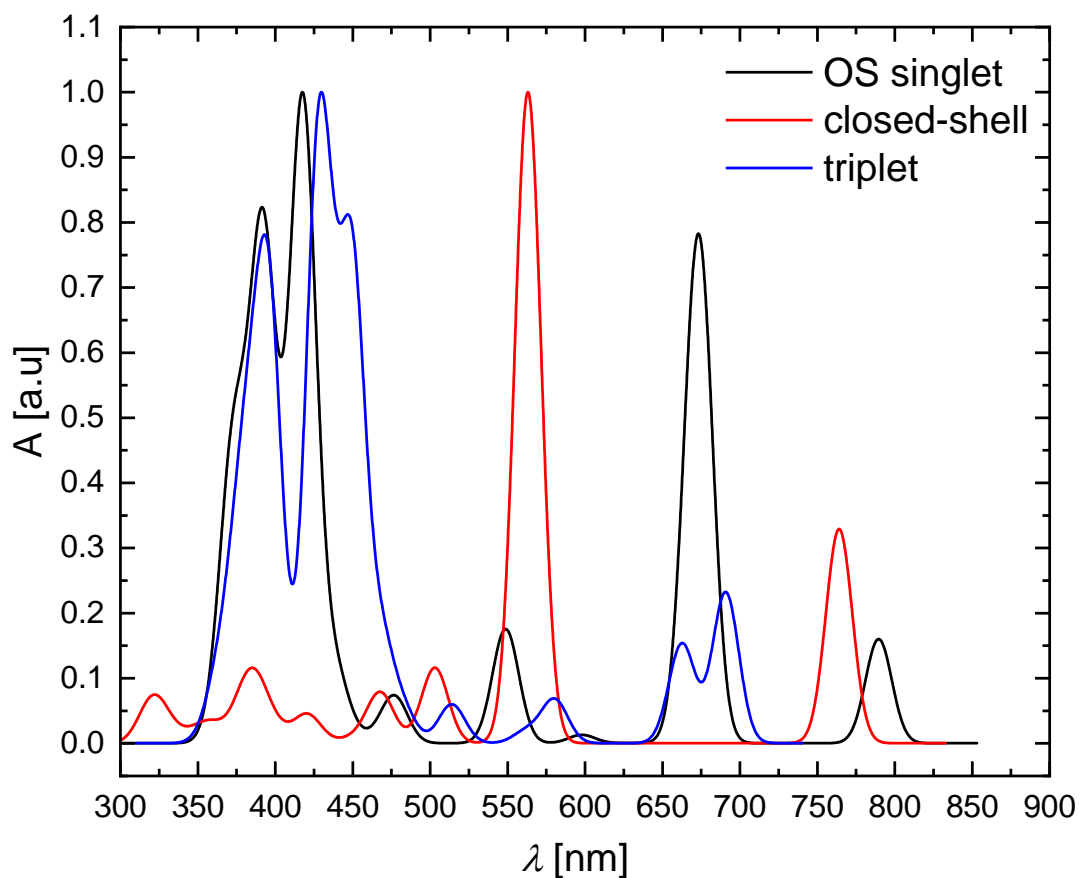
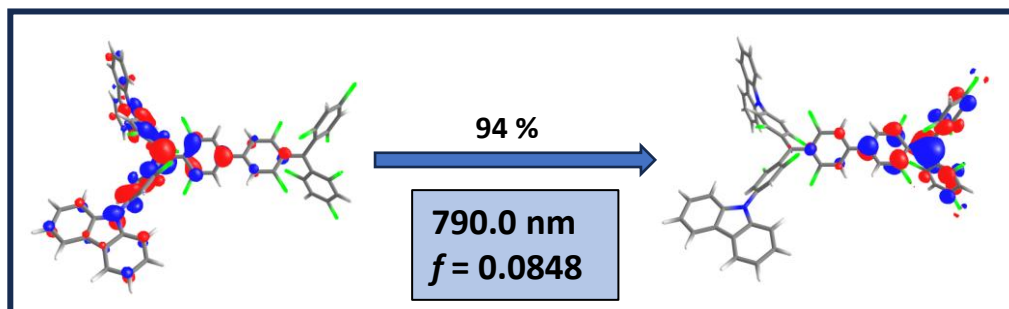
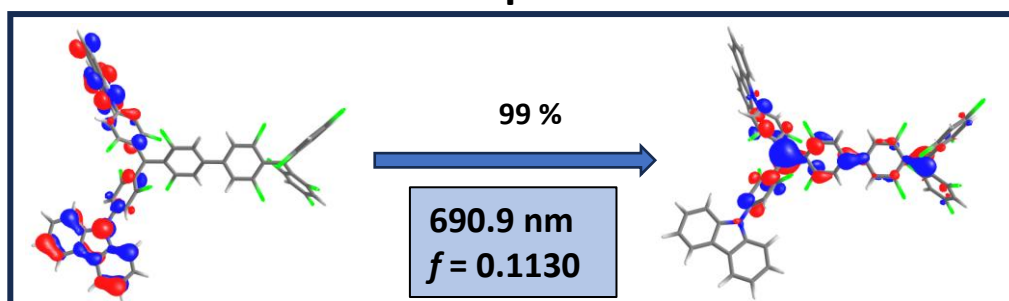


Figure S23 TD-DFT calculated UV-Vis absorption spectra of **1**.

Open-Shell Singlet



Triplet



Closed-Shell

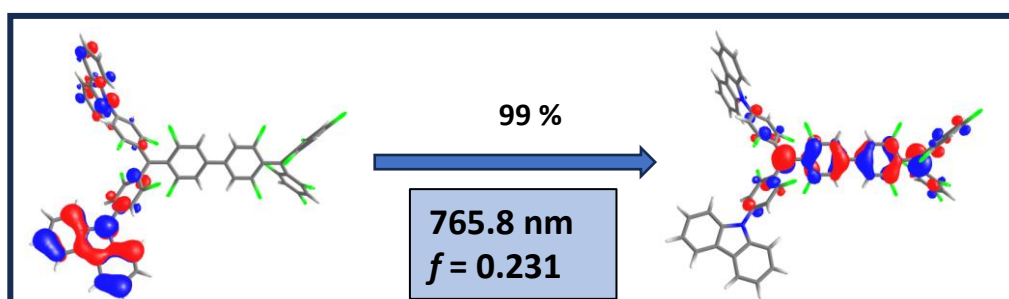


Figure S24 Natural transition orbitals of the lowest energy transitions (UV-Vis region) during absorption of **1** in open-shell singlet state, triplet state, and closed-shell state calculated by TD-DFT methods ((U)B3LYP-D3/def2-SVPD) obtained from geometry optimized structure of **1**.

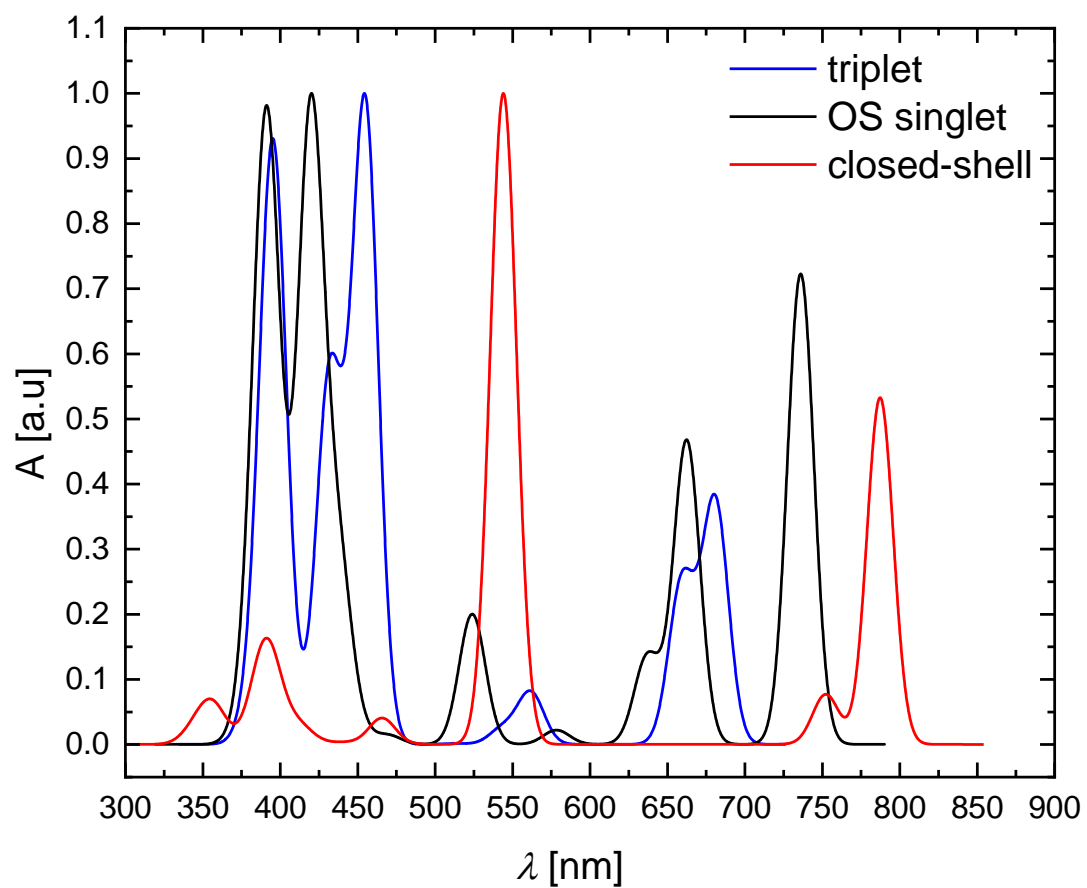
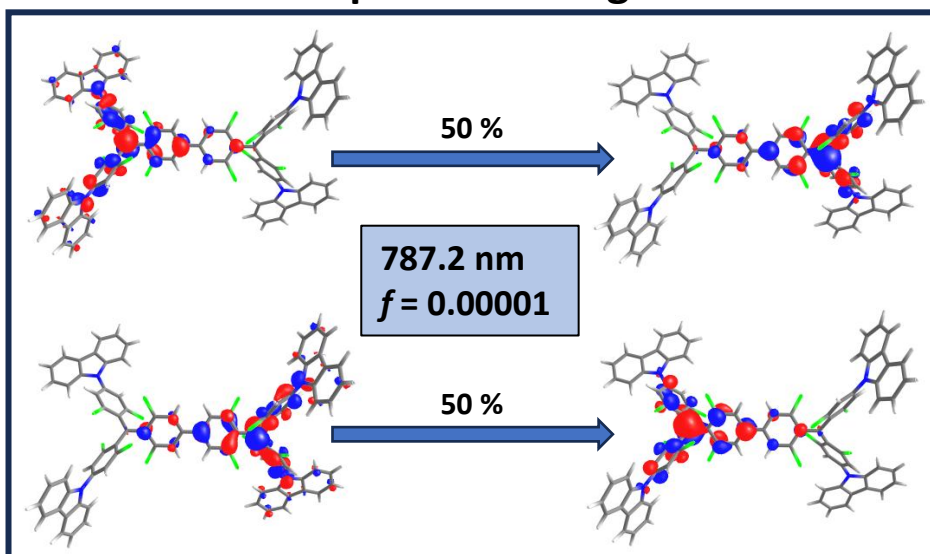
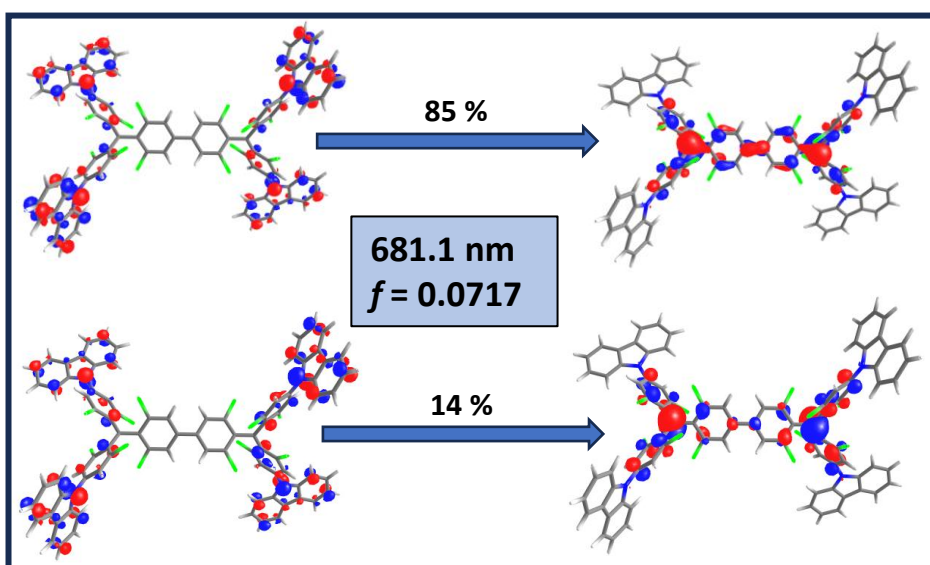


Figure S25 TD-DFT calculated UV-Vis absorption spectra of **2**.

Open-Shell Singlet



Triplet



Closed-shell

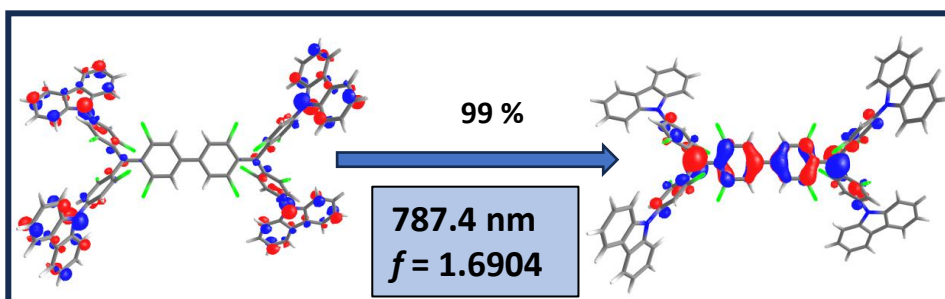


Figure S26 Natural transition orbitals of the lowest energy transitions (UV-Vis region) during absorption of **2** in open-shell singlet state, triplet state, and closed-shell state calculated by TD-DFT methods ((U)B3LYP-D3/def2-SVPD) obtained from geometry optimized structure of **2**.

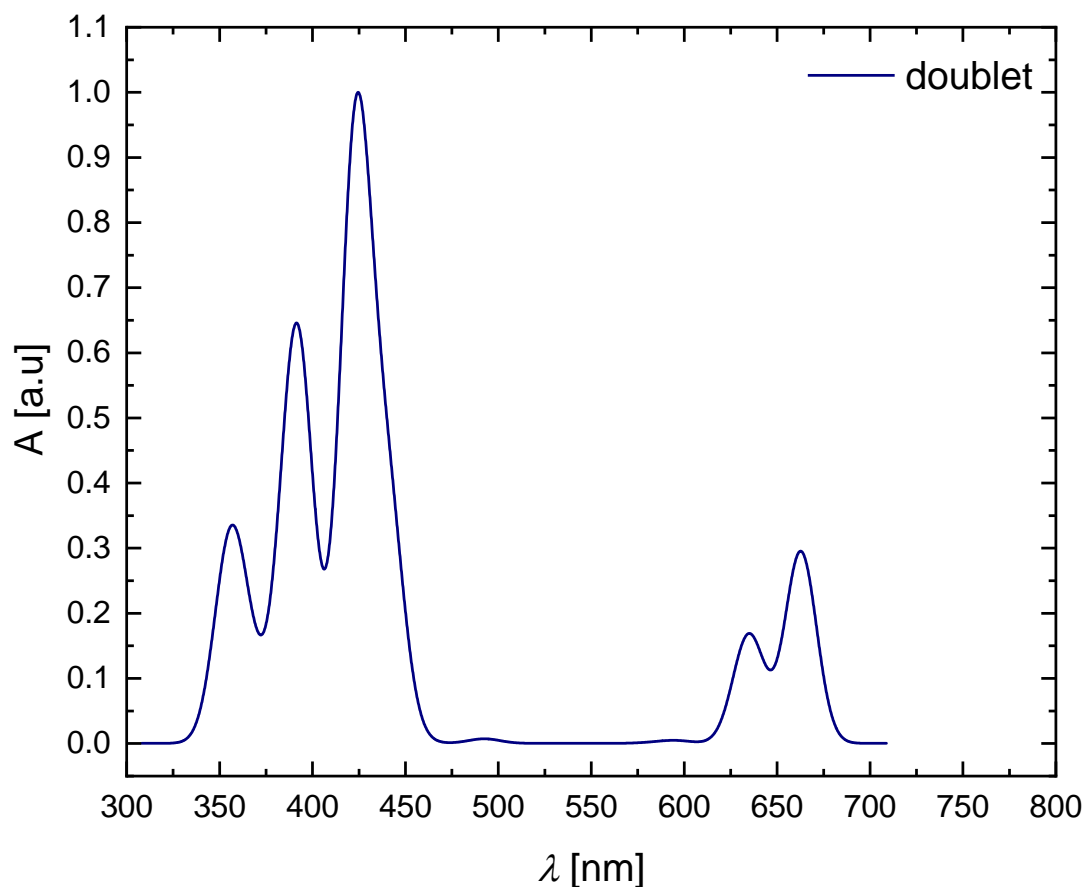


Figure S27 TD-DFT calculated UV-Vis absorption spectra of **3**.

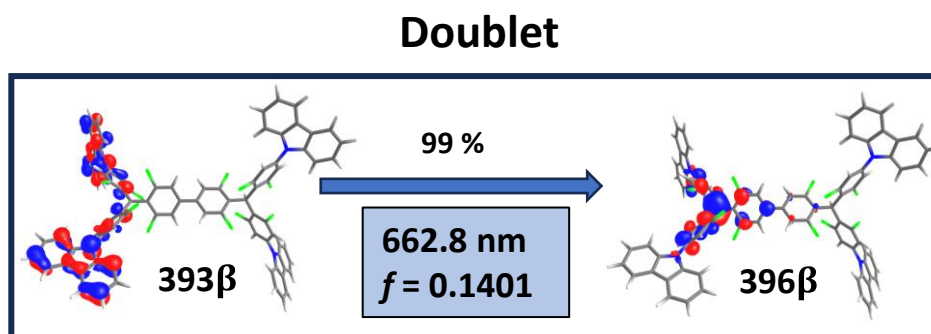


Figure S28 Natural transition orbitals of the lowest energy transition (UV-Vis region) during absorption of **3** in doublet state calculated by TD-DFT methods ((U)B3LYP-D3/def2-SVPD) obtained from geometry optimized structure of **3**.

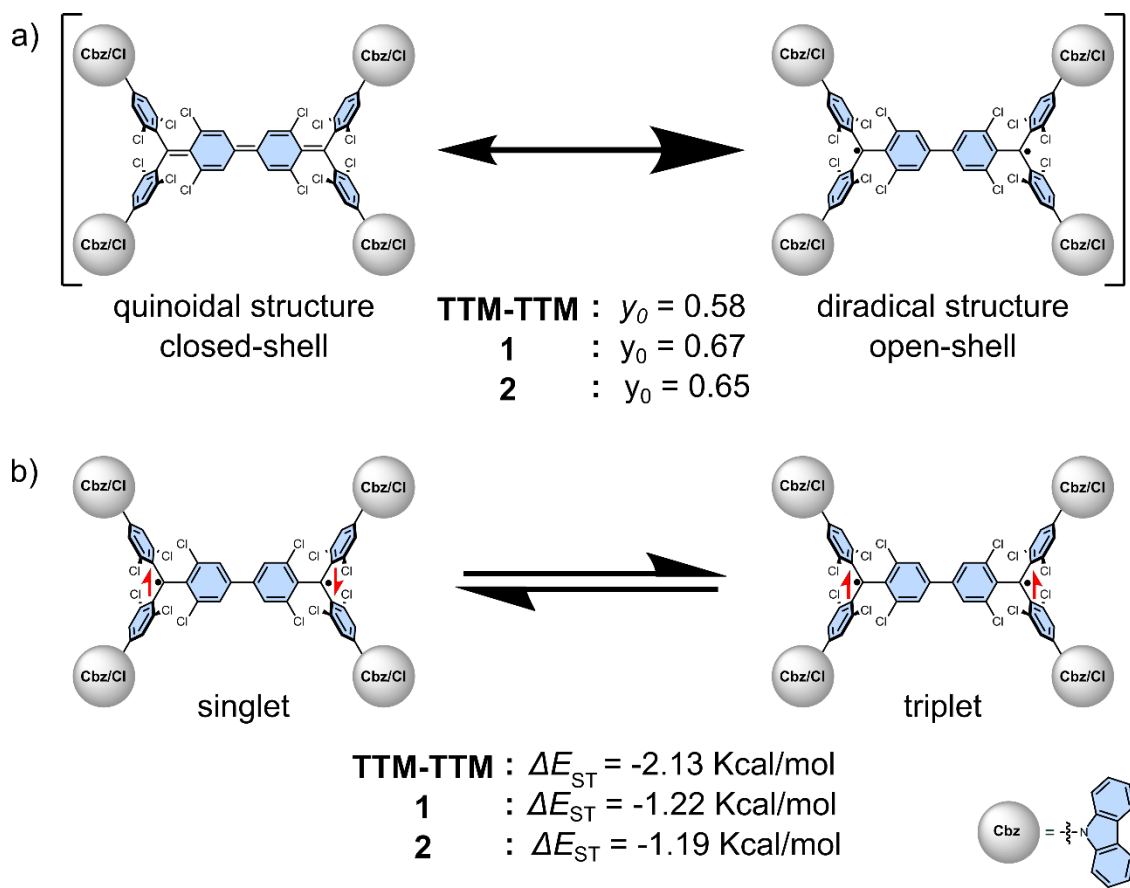


Figure S29 a) Resonance structures and their diradical character (y_0) (open/closed shell structure) b) Two possible spin state (singlet/triplet) with corresponding energies.

7. EPR measurements

To study the magnetic properties, a EPR measurements of **Cbz₂-TTM-I**, **1**, **2** and **3** in toluene, and for diradical **2**, and **3** in powder a VT-EPR were conducted. Analysis and Spectral fits were carried out similar with the previous report from our group.⁸

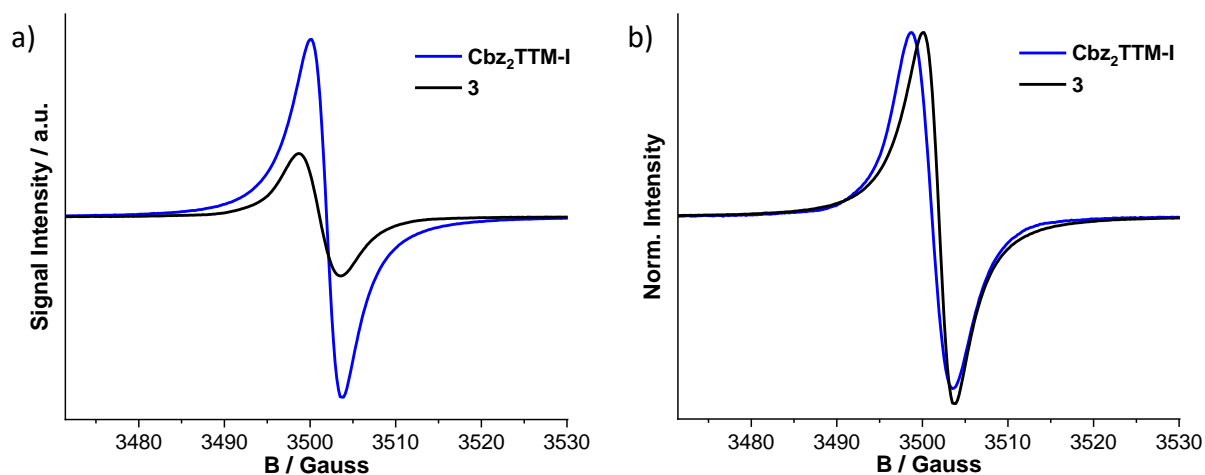


Figure S30 a) EPR spectrum b) Normalized EPR spectrum of **Cbz₂-TTM-I** and **3** in toluene at room temperature (296 K), for concentrations 0.33 mg/mL.

Table S5 Fitted parameters to the VT-EPR data shown in Figure 4c and 4d.

Compound	TTM-TTM	1	2
$\Delta E_{ST}/k_B$ (K)	-1565 ± 271	-805 ± 20	-662 ± 18
B (offset)	0.019 ± 0.001	0.02 ± 0.004	0.012 ± 0.007

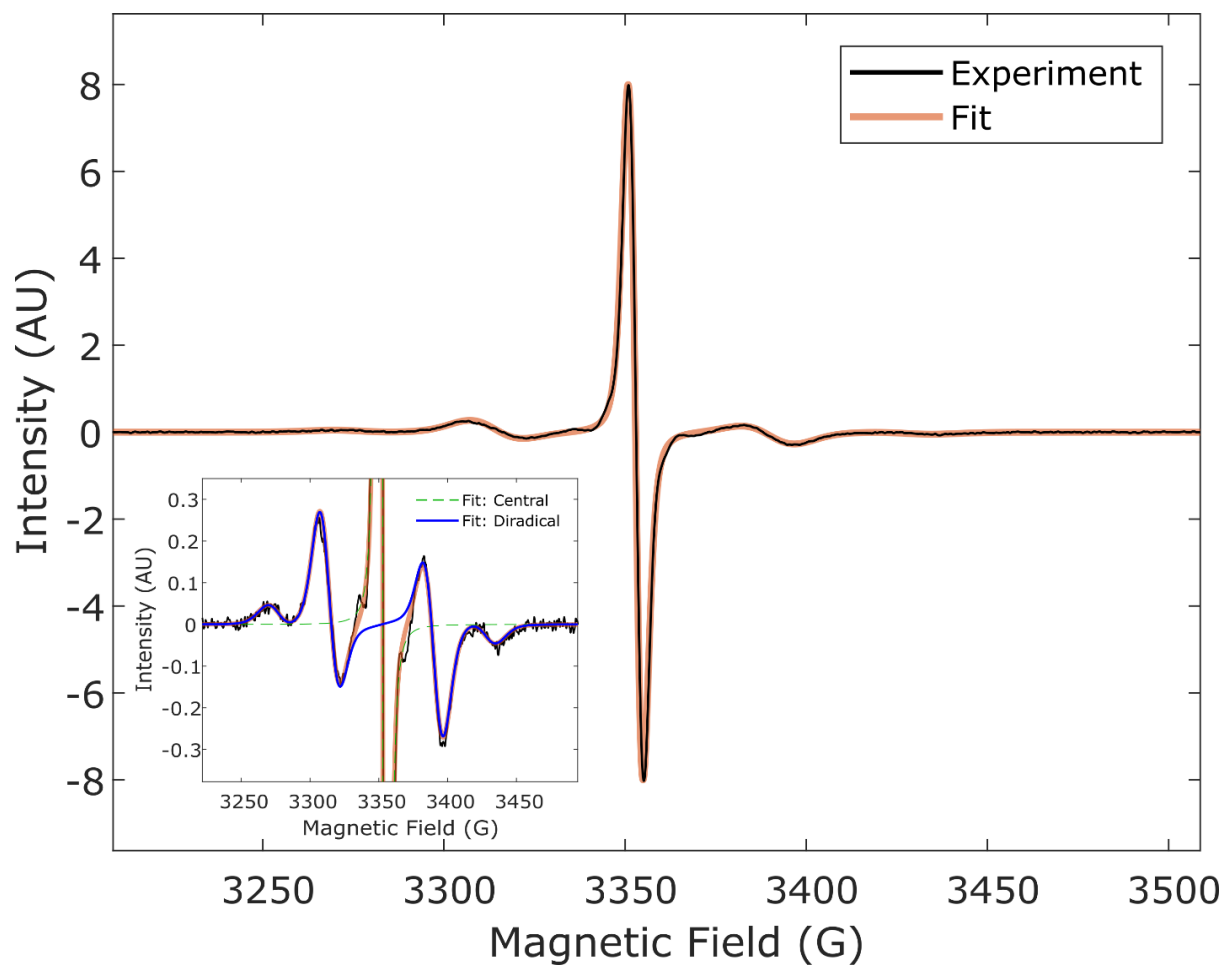


Figure S31 EPR spectrum of **1** in toluene (0.33 mg/mL) at $T=190$ K (black line) and spectral fit (red line). Inset shows zoom spectra and the decomposition of the fitted curve into individual contributions, central peak and diradical, shown as green dashed line and thick blue line, respectively. The fit yields, for the diradical, $|D| = 246$ MHz and a rotational correlation time $t_{\text{corr}} = 31$ ns. The acquisition was taken at the microwave frequency $\nu=9.41$ GHz, at the microwave power $P=300$ μW .

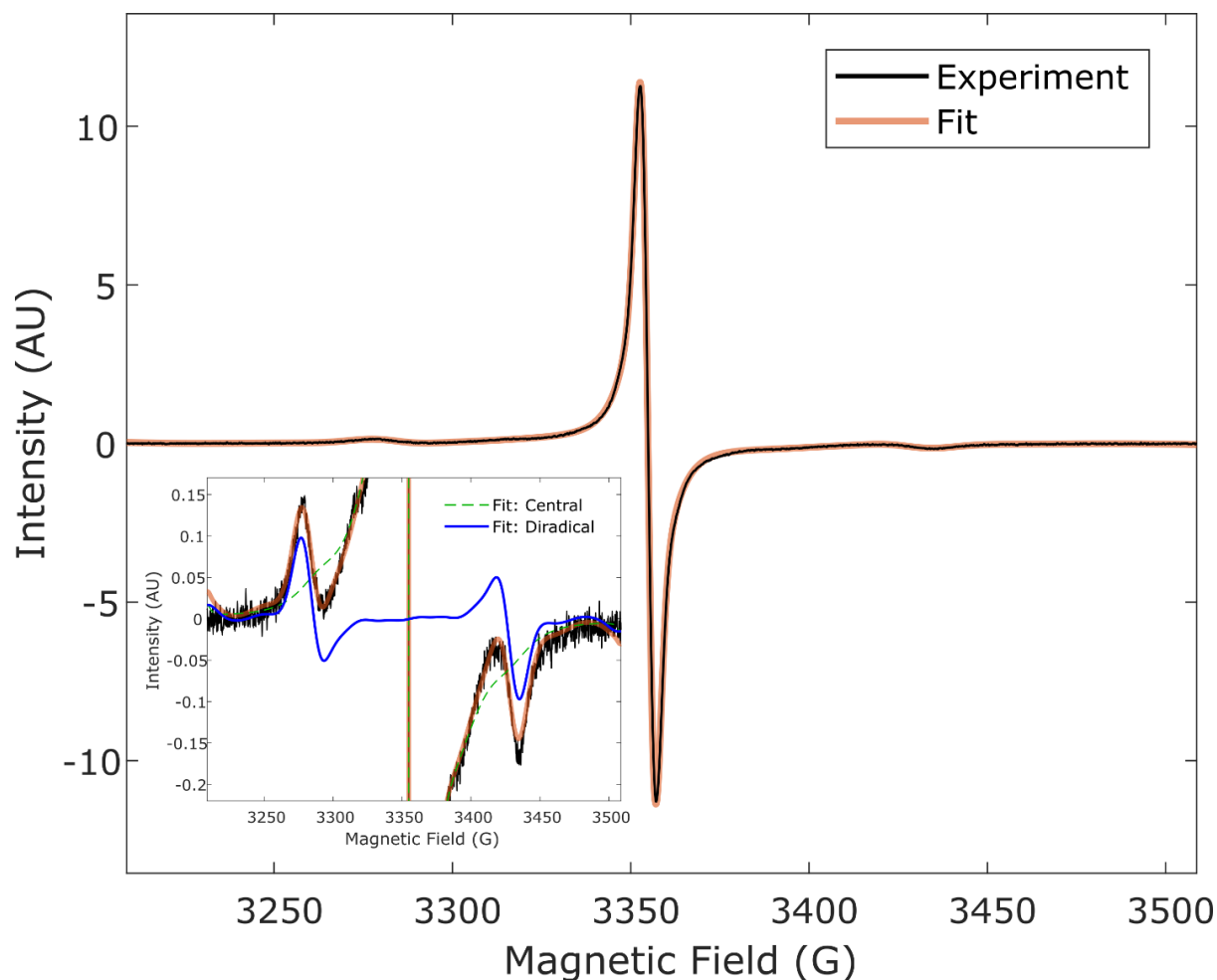


Figure S32 EPR spectrum of **2** in toluene (0.33 mg/mL) at $T=190$ K (black line) and spectral fit (red line). Inset shows zoom spectra and the decomposition of the fitted curve into individual contributions, central peak and diradical, shown as green dashed line and thick blue line, respectively. The fit yields, for the diradical, $|D| = 437$ MHz and a rotational correlation time $t_{\text{corr}} = 54$ ns. The acquisition was taken at the microwave frequency $\nu=9.41$ GHz, at the microwave power $P=300$ μ W.

Table S6 Fitted parameters to the EPR data shown in Figure S31 and S32.

Compound	$ D $ (MHz)	$\log t_{\text{corr}}$	t_{corr} (ns)
1	246 ± 2	-7.51 ± 0.06	31 ± 4
2	437 ± 2	-7.26 ± 0.06	54 ± 8

8. Supplementary NMR and mass spectra

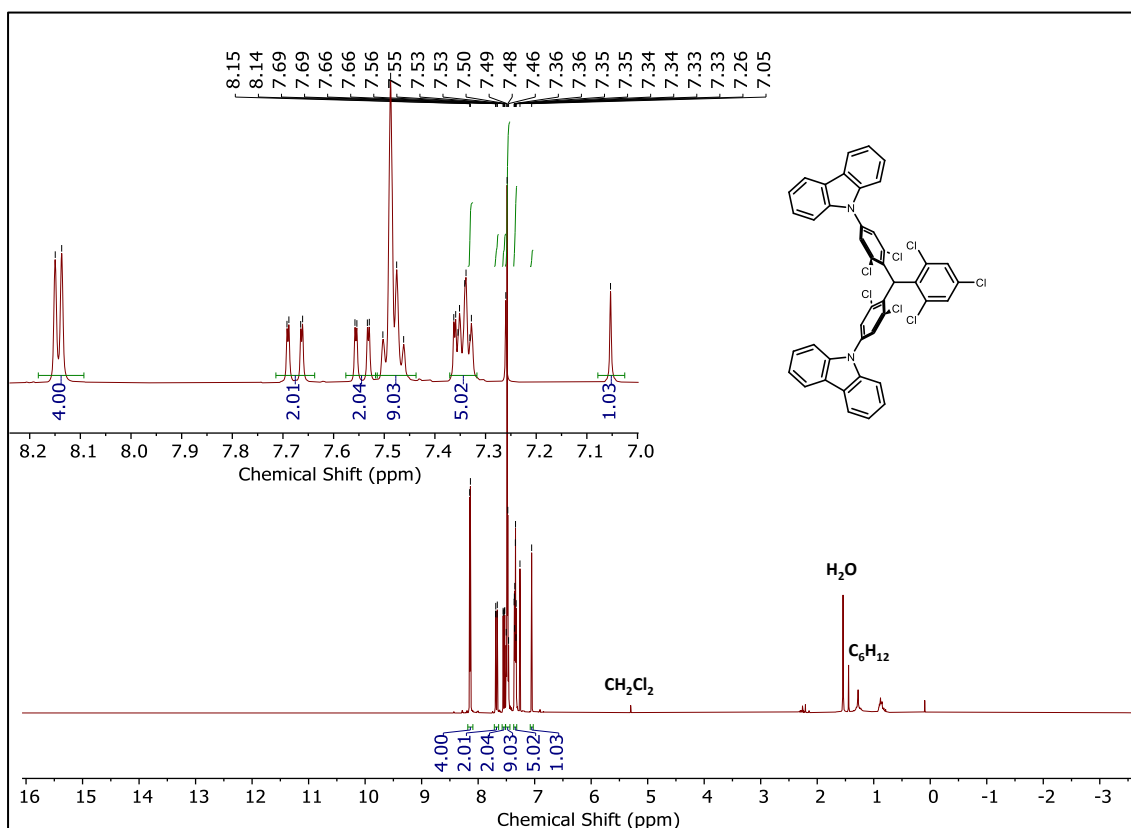


Figure S33 ^1H NMR of **Cbz₂-HTTM** in CDCl_3 at 298 K.

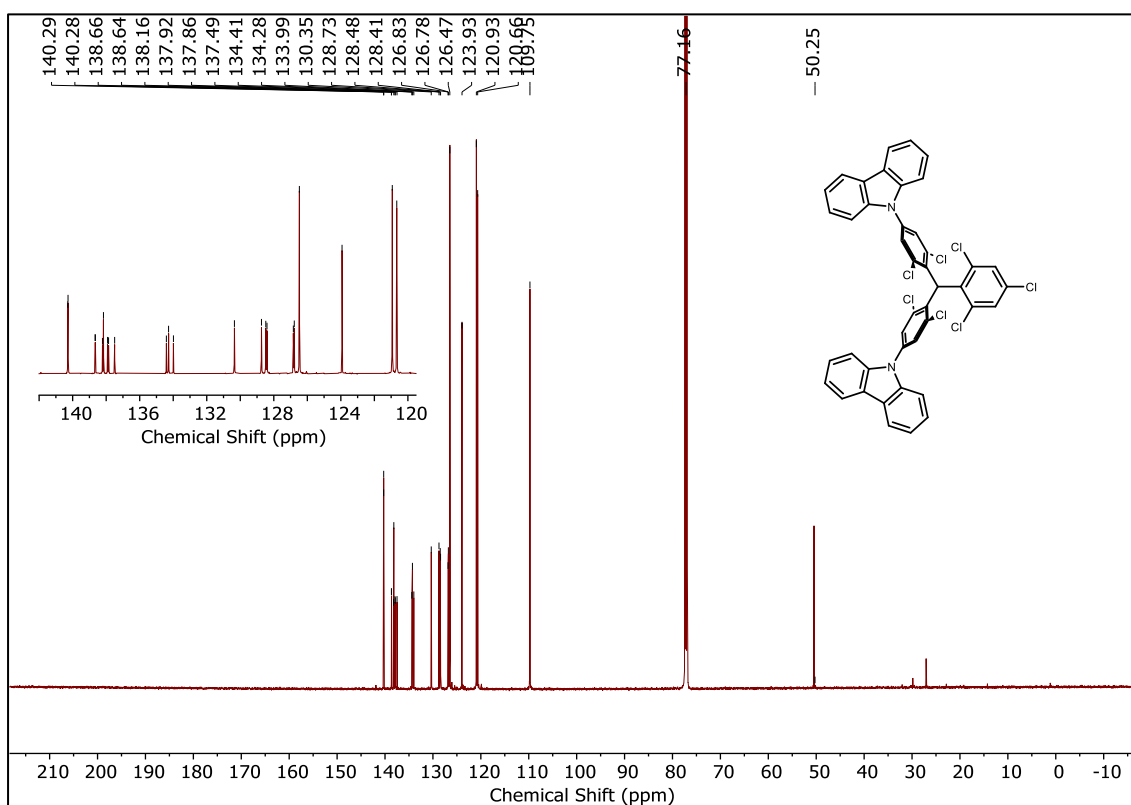


Figure S34 ^{13}C $\{^1\text{H}\}$ NMR of **Cbz₂-HTTM** in CDCl_3 at 298 K.

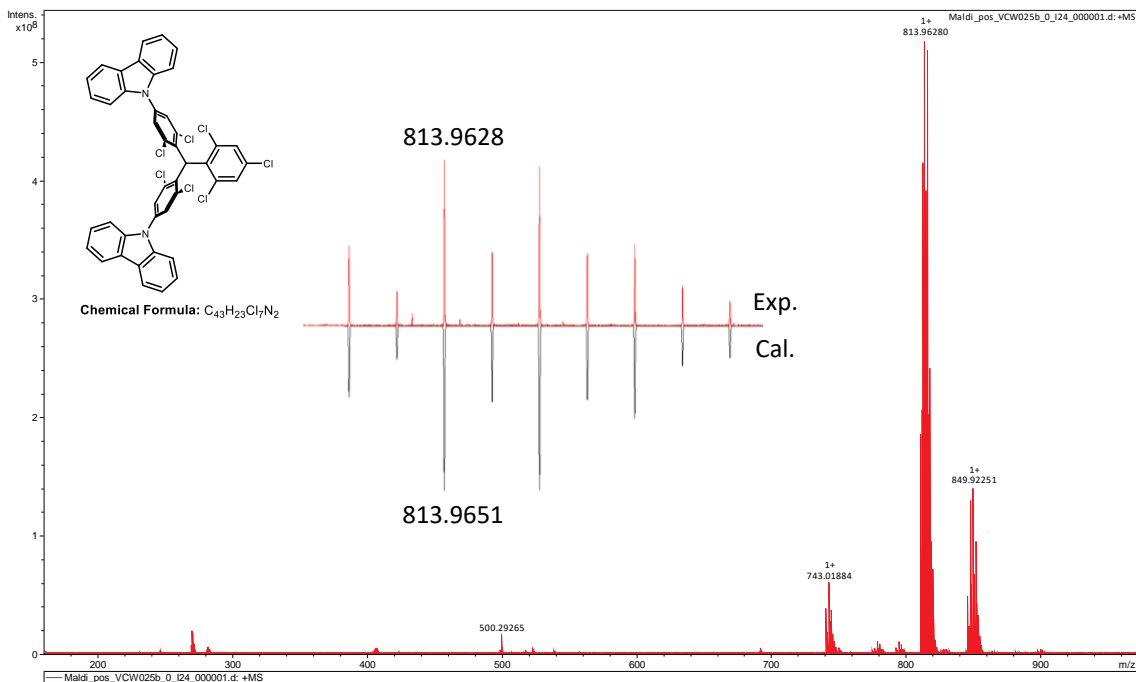


Figure S35 MALDI of Cbz₂-HTTM.

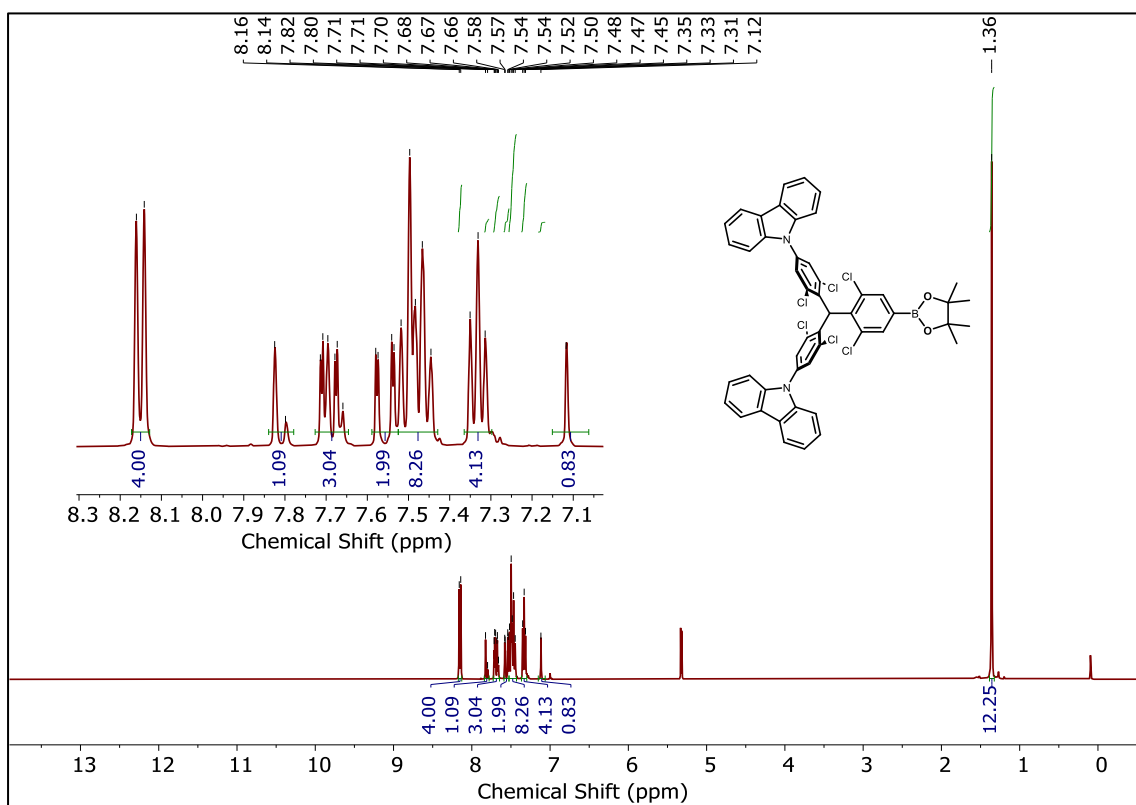


Figure S36 ¹H NMR of Cbz₂-HTTM-Bpin in CD₂Cl₂ at 298 K.

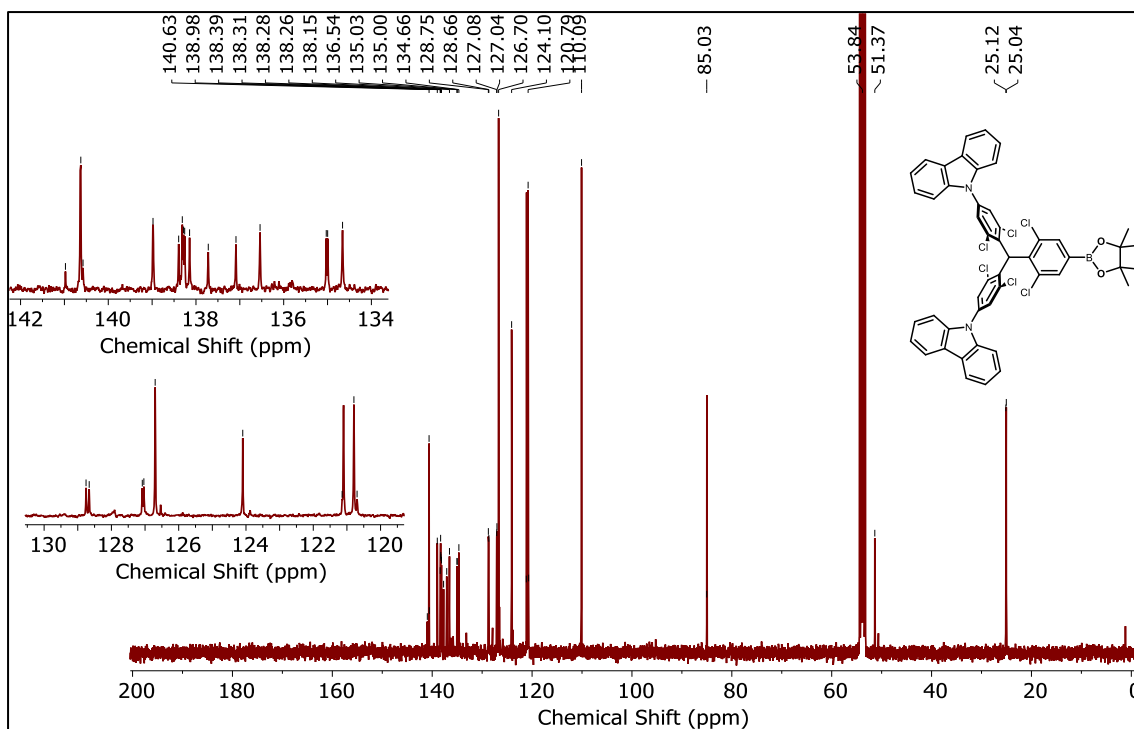


Figure S37 ^{13}C $\{^1\text{H}\}$ NMR of **Cbz₂-HTTM-Bpin** in CD_2Cl_2 at 298 K.

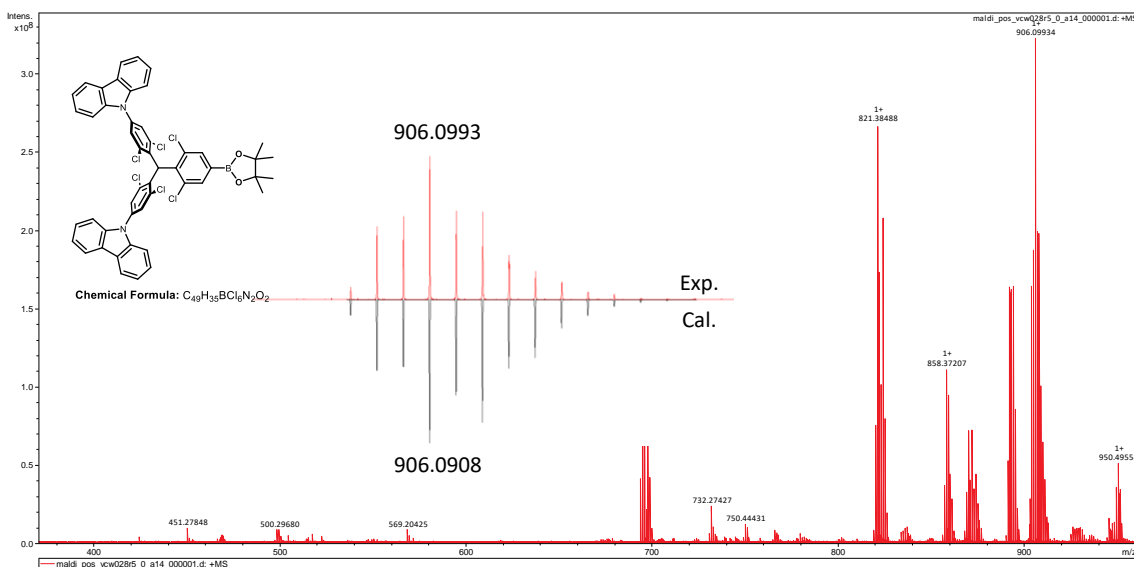


Figure S38 MALDI of **Cbz₂-HTTM-Bpin**.

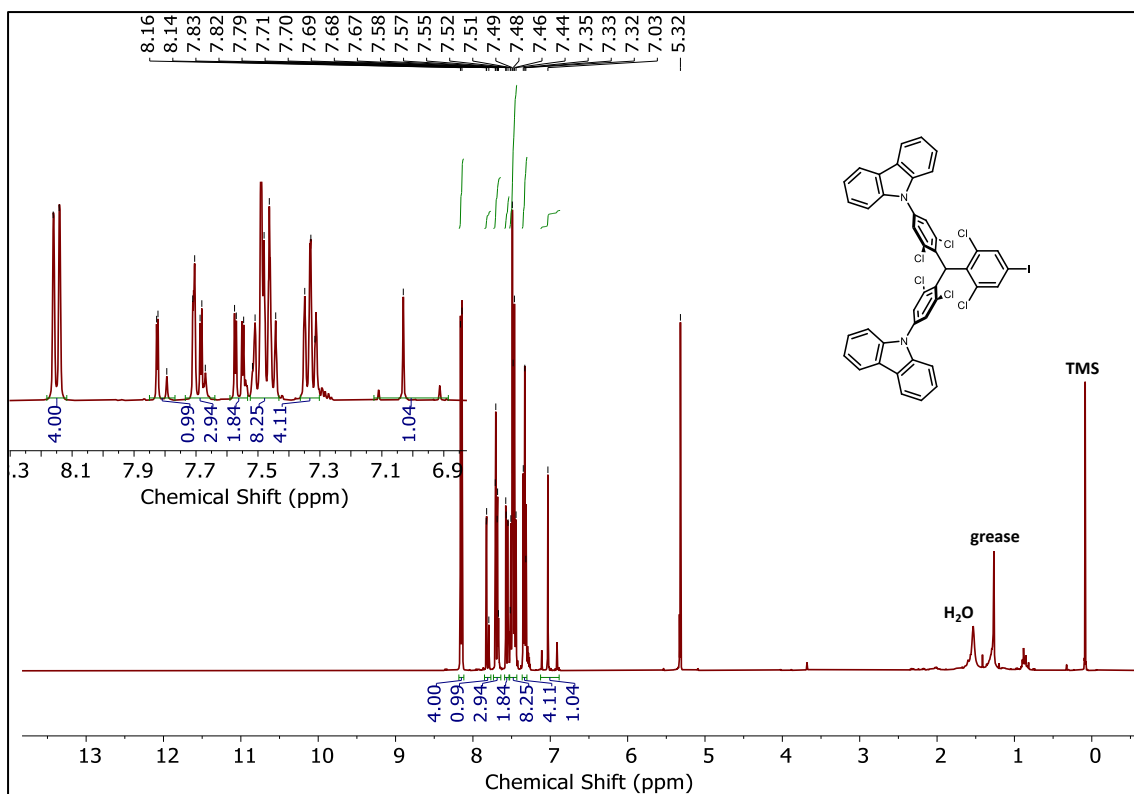


Figure S39 ¹H NMR of Cbz₂-HTTM-I in CD₂Cl₂ at 298 K.

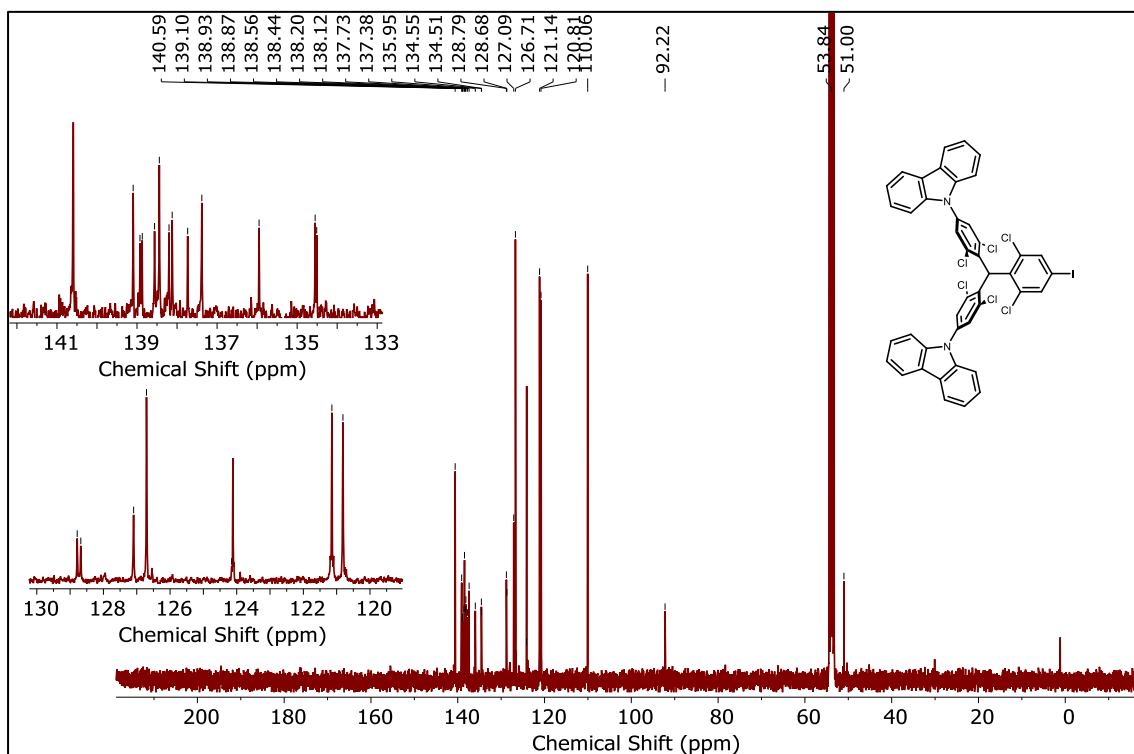


Figure S40 ¹³C {¹H} NMR of Cbz₂-HTTM-I in CD₂Cl₂ at 298 K.

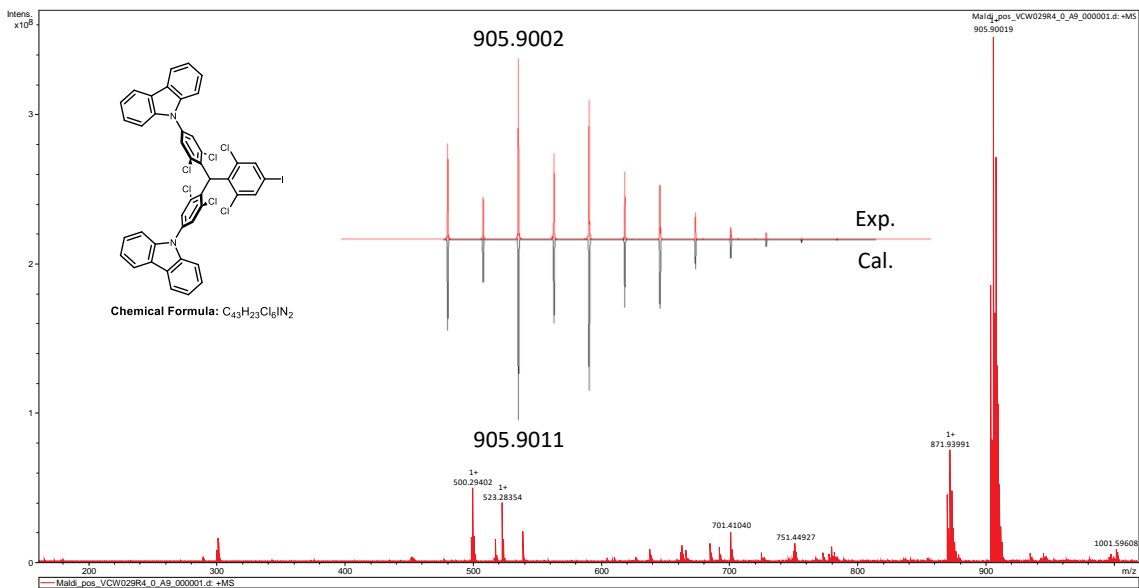


Figure S41 MALDI of Cbz₂-HTTM-I.

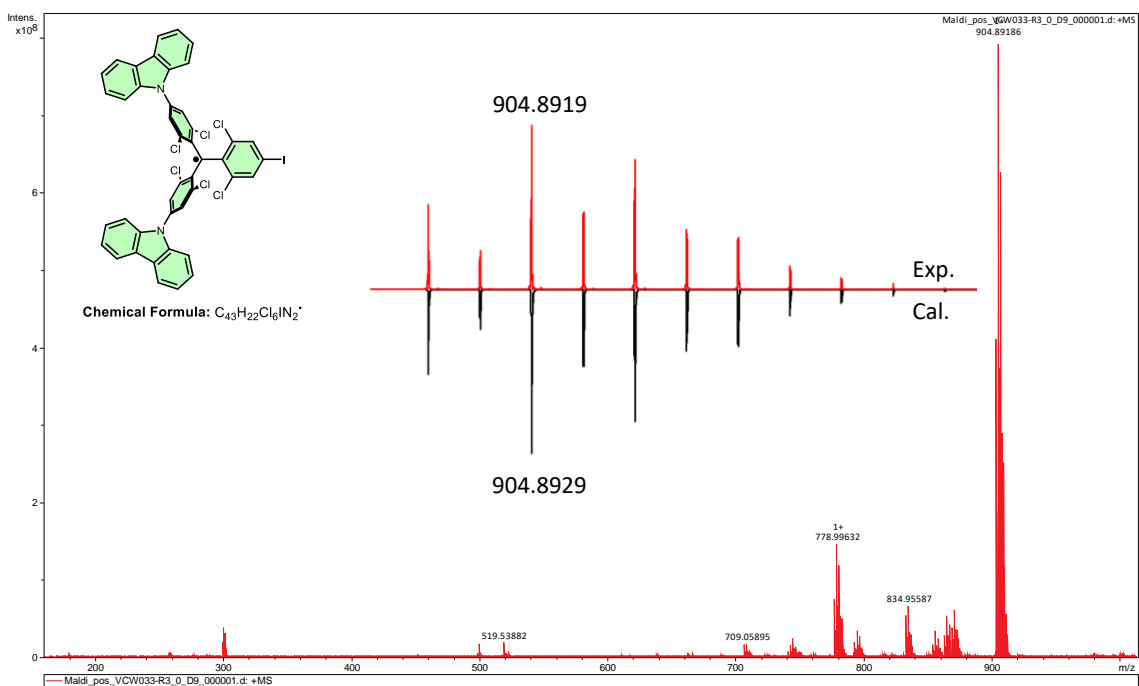


Figure S42 MALDI of Cbz₂-TTM-I.

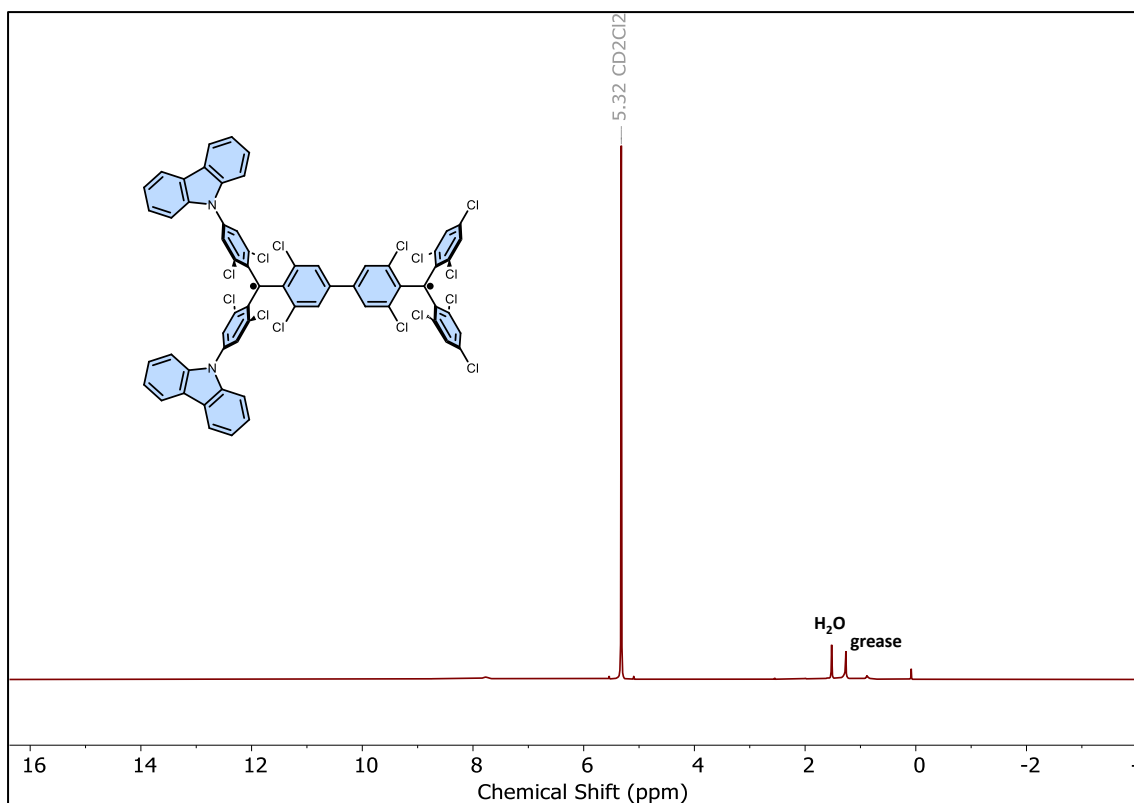


Figure S43 ^1H NMR of **1** in CD_2Cl_2 at 298 K.

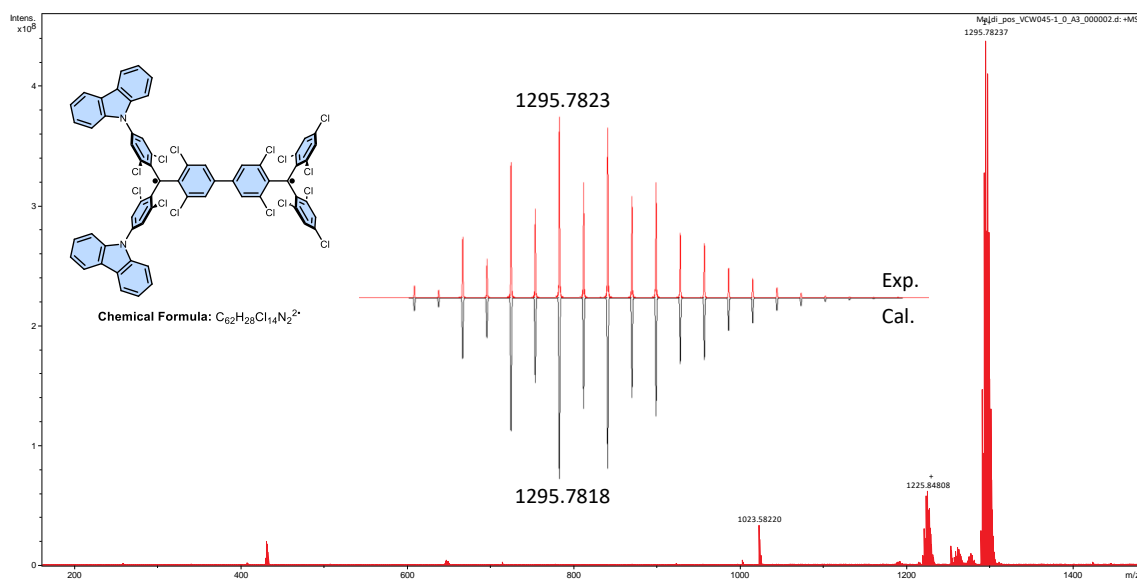


Figure S44 MALDI of **1**.

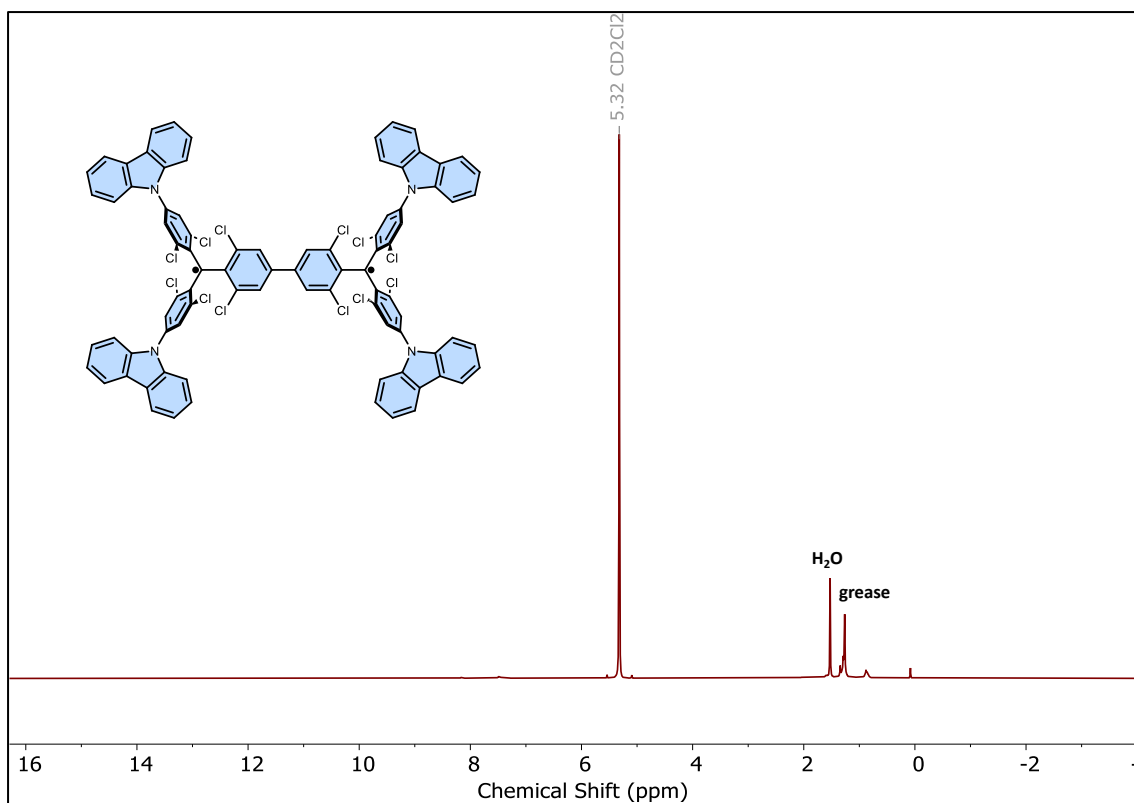


Figure S45 ^1H NMR of **2** in CD_2Cl_2 at 298 K.

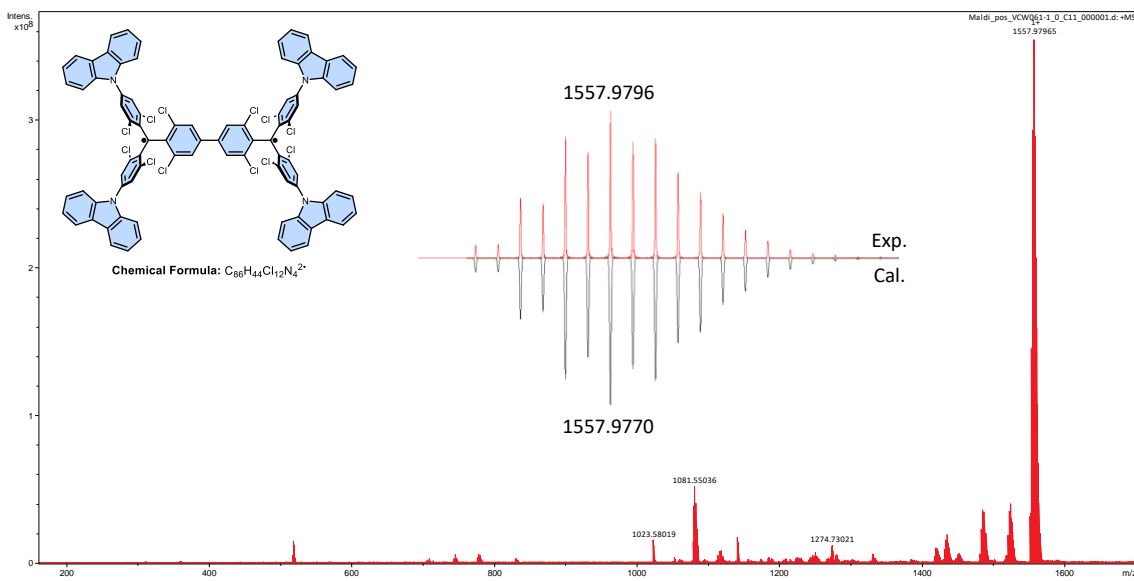


Figure S46 MALDI of **2**.

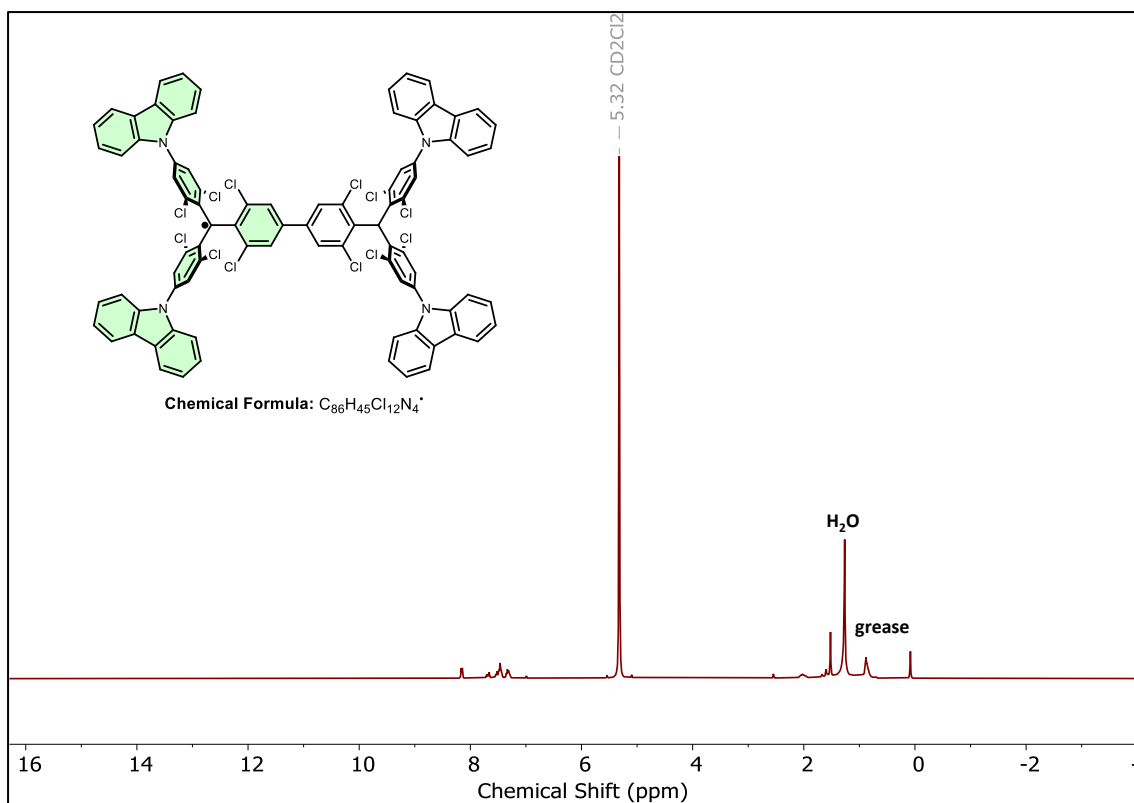


Figure S47 ¹H NMR of **3** in CD₂Cl₂ at 298 K.

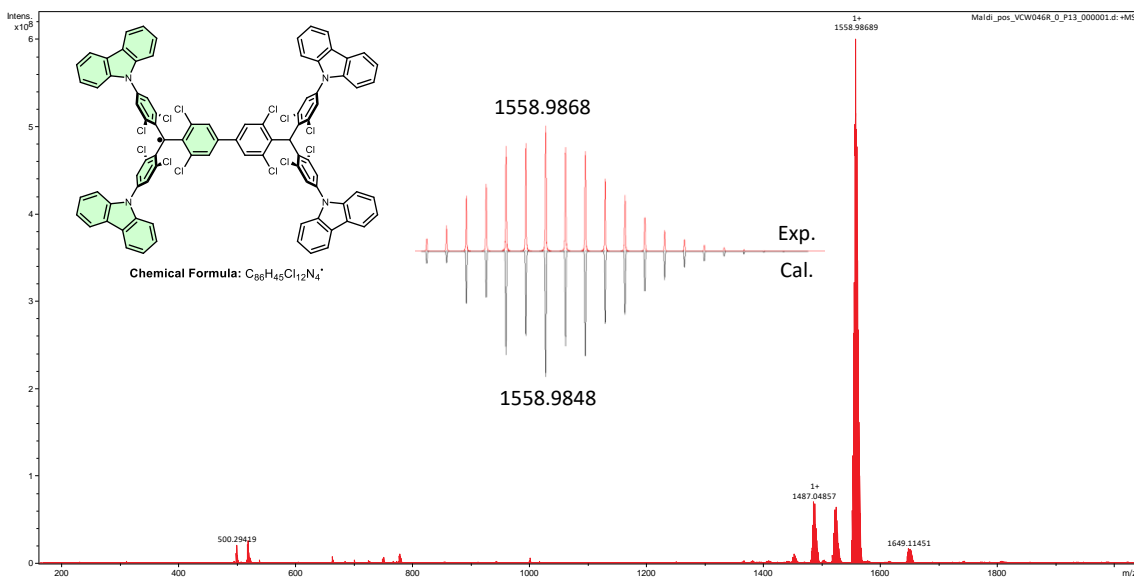


Figure S48 MALDI of **3**.

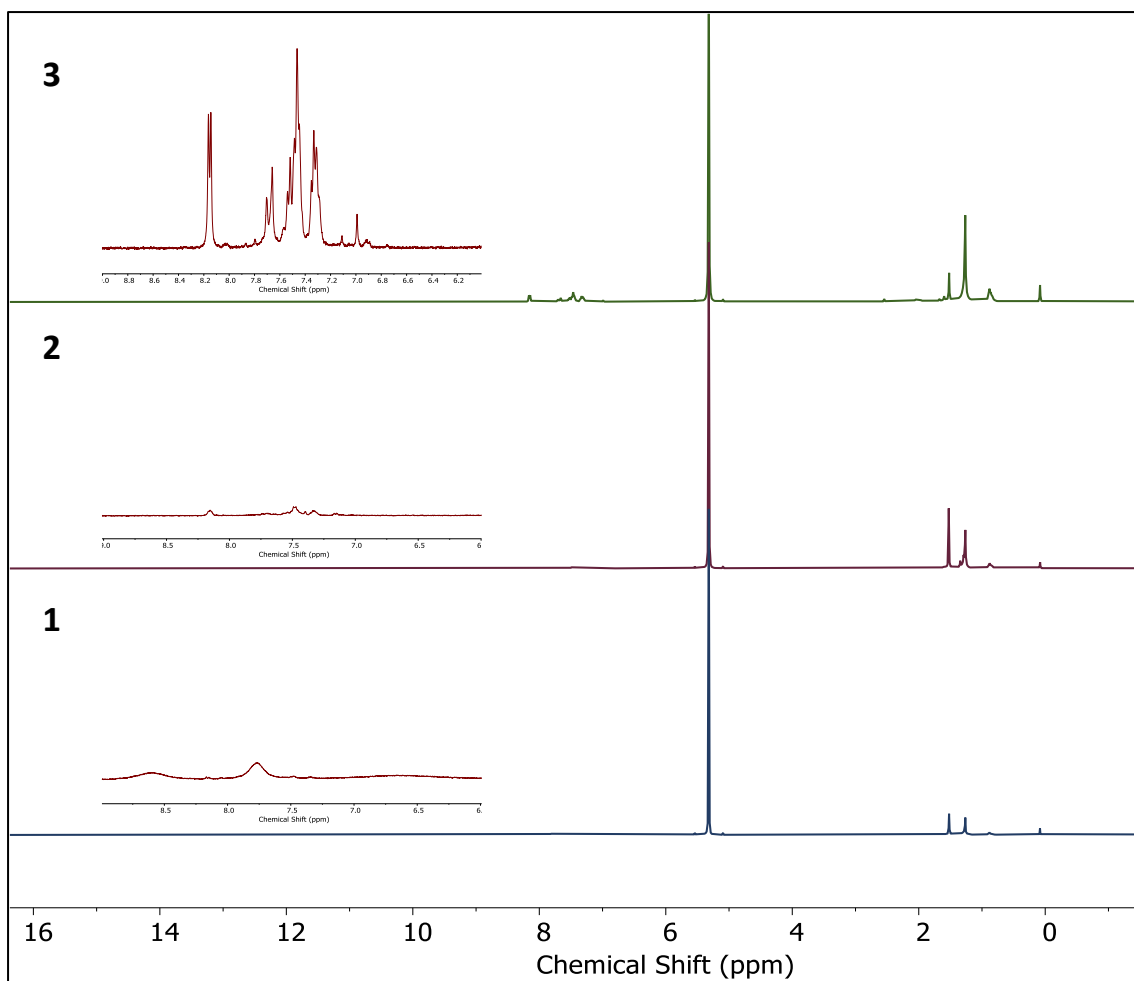


Figure S49 Stacked ¹H NMR of **1**, **2** and **3** in CD₂Cl₂ at 298 K.

9. References

1. (a) M. E. Arnold, L. Roß, P. Thielert, F. Bartley, J. Zolg, F. Bartsch, L. A. Kibler, S. Richert, C. Bannwarth and A. J. C. Kuehne, *Adv. Opt. Mater.*, 2024, **12**, 2400697; (b) M. E. Arnold and A. J. C. Kuehne, *Dyes Pigm.* **2023**, *208*, 110863.
2. S. Castellanos, D. Velasco, F. López-Calahorra, E. Brillas and L. Julia, *J. Org. Chem.*, 2008, **73**, 3759–3767.
3. F. Neese, *WIREs Comput. Mol. Sci.* 2022, **12**, e1606.
<https://doi.org/10.1002/wcms.1606>.
4. (a) F. Weigend, *Phys. Chem. Chem. Phys.* 2006, **8**, 1057-1065; (b) F. Weigend and R. Ahlrichs, *Phys. Chem. Chem. Phys.* 2005, **7**, 3297-3305; (c) S. Grimme, J. Antony, S. Ehrlich and H. Krieg, *J. Chem. Phys.* 2010, **132**, 154104; (d) S. Grimme, S. Ehrlich and L. Goerigk, *J. Comput. Chem.* 2011, **32**, 1456-1465.
5. D. Rappoport, and F. Furche, *J. Chem. Phys.* 2010, **133**, 134105.
6. (a) K. Yamaguchi, Y. Takahara and T. Fueno, *Applied Quantum Chemistry* (Dordrecht) 1986, 155- 184; (b) T. Soda, Y. Kitagawa, T. Onishi, Y. Takano, Y. Shigeta, H. Nagao, Y. Yoshioka, and K. Yamaguchi *Chem. Phys. Lett.* 2000, **319**, 223-230.
7. K. Yamaguchi, *Chem. Phys. Lett.* 1975, **33**, 330-335.
8. X. Chang, M. E. Arnold, R. Blinder, J. Zolg, J. Wischnat, J. van Slageren, F. Jelezko, A. J. C. Kuehne and M. von Delius, *Angew. Chem. Int. Ed.*, 2024, **63**, e202404853.
9. K. Karon and M. Lapkowski, *J. Solid State Electrochem.*, 2015, **19**, 2601–2610.
10. S. H. Hsiao and S. W. Lin, *Polym. Chem.*, 2016, **7**, 198-211.